Technical report submitted to UGC Major Research Project

Detection of Mines, Submarines and Mapping of Obstacles using Image Processing for Secured Patrolling of Sea Coast

UGC Major Research project sanction **F. No. 43-310/2014(SR) dated 07-01-2016**

(Technical report No. AITAM/ECE/UGC/Major Res proj/ MNVSSK/2018/Oct/2)

Dr. M N V S S Kumar

Principal Investigator

Department of Electronics & Communication Engineering

Aditya Institute of Technology and Management (A)

Tekkali, Srikakulam-532201, A.P., India

PROFORMA FOR SUBMISSION OF INFORMATION AT THE TIME OF SENDING THE FINAL REPORT OF THE WORK DONE ON THE PROJECT

1. **TITLE OF THE PROJECT:** Detection of Mines, Submarines and Mapping of Obstacles using Image Processing for Secured Patrolling of Sea Coast
2. **NAME AND ADDRESS OF THE PRINCIPAL INVESTIGATOR:**
   Dr. M N V S S Kumar
   Aditya Institute of Technology and Management (A)
   Tekkali, Srikakulam-532201, A.P., India
3. **NAME AND ADDRESS OF THE INSTITUTION:**
   Aditya Institute of Technology and Management (A)
   Tekkali, Srikakulam-532201, A.P., India
4. **UGC APPROVAL LETTER NO. AND DATE:** 43-310/2014(SR) dated 07-01-2016
5. **DATE OF IMPLEMENTATION:** 1st July, 2015
6. **TENURE OF THE PROJECT:** 3 Years
7. **TOTAL GRANT ALLOCATED:** Rs. 4,26,000/-
8. **TOTAL GRANT RECEIVED:** Rs. 4,17,000/-
9. **FINAL EXPENDITURE:** Rs. 4,26,543/-
10. **TITLE OF THE PROJECT:** Detection of Mines, Submarines and Mapping of Obstacles using Image Processing for Secured Patrolling of Sea Coast
11. **OBJECTIVES OF THE PROJECT:** Attached
12. **WHETHER OBJECTIVES WERE ACHIEVED:** Yes
13. **ACHIEVEMENTS FROM THE PROJECT:** Attached
14. **SUMMARY OF THE FINDINGS:** Attached
15. **CONTRIBUTION TO THE SOCIETY:** Attached
16. **WHETHER ANY PH.D. ENROLLED/PRODUCED OUT OF THE PROJECT:** No
17. **NO. OF PUBLICATIONS OUT OF THE PROJECT:** 3

SIGNATURE OF THE PRINCIPAL INVESTIGATOR **REGISTRAR/PRINCIPAL**

Annual Report of the work done on the Major Research Project

Project report No. **:** 2

UGC Reference No. F. **:** 43-310/2014(SR) dated 07-01-2016

Period of report **:** July 2015 to July 2018 (3 Years)

Title of the Research Project **:** Detection of Mines, Submarines and Mapping of Obstacles using Image Processing for Secured Patrolling of Sea Coast

Principal Investigator (PI) **:** Dr. M N V S S Kumar

Department **:** Electronics & Communication Engineering

Institutional Address **:** Aditya Institute of Technology and Management (A) Tekkali, Srikakulam-532201, A.P., India

Effective date of starting of the project: 1st July, 2015

Grant approved and expenditure incurred during the period of the report:

- **a. Total amount approved** **:** Rs. 4,26,000/-
- **b. Total expenditure** **:** Rs. 4,26,543/-

Report of the work done:

i. **Brief objective of the project** **:** Report Attached
ii. **Work done so far and results achieved and publications, if any, resulting from the work** **:** Report Attached
iii. **Has the progress been according to original plan of work and towards achieving the objective. if not, state reasons** **:** Yes
iv. **Please indicate the difficulties, if any, experienced in implementing the project:** No
v. **If project has not been completed, please indicate the approximate time by which it is likely to be completed:** Completed
vi. **If the project has been completed, please enclose a summary of the findings of the study:** Yes
vii. **Any other information which would help in evaluation of work done on the project:** No

SIGNATURE OF THE PRINCIPAL INVESTIGATOR **REGISTRAR/PRINCIPAL**

Objectives of the Project

- Investigation of various underwater and terrestrial navigational aids and analysis of the propagation characteristics of sonar signals under the influence of underwater noise.
- Analysis of chirp technology and Monotonic sonars in terms of range resolution with which separation of two objects can be identified clearly in the image obtained from the sonar.
- Analysis of the existing image segmentation schemes and their applicability to the sonar images.
- Development of a new Image Processing algorithm to identify the objects in the noisy underwater sonar images and comparison of its performance with existing segmentation methods.
- Development of a surface construction algorithm to construct the 3D shape of an underwater object from the 2D images obtained from the sonar.

Methodology

The first step in achieving the research goal is the acquisition and processing of images generated by the Imaging sonar. The images that are received from the imaging sonar provide only the range and bearing of the objects. These objects are required to be detected in the image frames received from the sonar. This involves the processing of the images in such a way that the detection of real objects is not missed out and no false alarm is detected. The sonar images are required to be pre-processed and an image processing algorithm is to be developed which combines the features of segmentation methods. Segmentation is required to distinguish objects from the background noise. Several existing segmentation methods have to be implemented on sonar images. As sonar images are very difficult to process, further research is to be undertaken and a new image processing algorithm that suits the underwater real sonar images over the coast of India is to be designed and developed. As the sonar images are having lot of noise, it is necessary to analyze the filters to check the suitability to the sonar images before detecting the underwater object.

Once the image is segmented and the objects are detected, their features are to be extracted. The main aim of feature extraction is to extract the size and shape of the objects. The object detected from the sonar is a 2D which provides only range and bearing of the object. Though there are so many 3D surface construction algorithms like Ball Pivoting, Triangulation, Voroni etc., they are suitable only to terrestrial applications. So there is a need for the extraction of the underwater 3D shape from the 2D images obtained. So a new 3D surface reconstruction algorithm for extracting the 3D features of the underwater object is to be developed.

Technical Report

1. Introduction

Classification of underwater objects such as mines, floating objects, submarines and controlling of vessel traffic in all major ports along the sea coast has become a crucial factor and essential for all developing countries.

The crucial equipment that provides navigational and surveillance capability to the Autonomous Underwater Vehicle (AUV) is the sonar. SONAR **(So**und **Na**vigation and **R**anging) is a sensor that uses sound propagation, mounted onto the AUV to navigate, communicate and detect underwater mines. Sonar is the underwater equivalent of Radar and its functions are many and varied. These include detection, identification, location and speed indication of the 'targets of interest'. Radar operates on the principle of transmitting and/or receiving electromagnetic waves, travelling at approximately the speed of light ($3x10^8$ meters/sec) through space or the atmosphere. Sonar, on the other hand, relies on acoustic energy in seawater which travels at 1,500 meter/sec, depending upon conditions such as temperature, depth, and salinity. There are basically two modes of operation of sonar: 'Passive' and 'Active'. A passive sonar system emits no signals. Active sonar employs a transmitter to send out sound pulses and a receiver to record returning echoes. In conventional active sonars, when the separation of the targets is less than the range resolution, then it displays a single large combined target rather than multiple smaller targets. Compressed High Intensity Radar Pulse (CHIRP) sonars are invented to overcome the limitations (i.e., the low coverage area and low range resolution) of conventional monotonic sonars. In this project, the images from the chirp sonar fitted on AUV are used for underwater object detection and tracking analysis.

In underwater navigation, timely scanning of area in front of the AUV and detection of objects is very important to avoid collision of AUV with vessels or underwater objects. With the advancement of technology, there are Imaging sonars which scan areas upto a range of 100 to 300 meters in front of the AUV and provide images as output. But the information that is available from these imaging sonars is limited to range and bearing only. Therefore, there is a clear need for extraction of features (range, bearing, size, shape and speed) of all underwater objects (that are coming in the way of an AUV) by making use of the information available in the images.

In addition, the sonar information collected while searching for, or identifying, underwater mines is often presented to the operator in the form of a two dimensional image. This 2D

information provides only range and bearing but not depth of the target. These 2D sonars cannot distinguish between the safe sea floor and the dangerous under water obstacles through depth measurement. They must rely on visual cues to guess whether or not the obstacles are located in the water column or on the sea floor. In order to overcome the problem, a new surface construction algorithm is developed, in which the complete 3D model of the object of interest can be extracted from the 2D images obtained from the sonar.

Object identification in the 2D images obtained from sonar is very important for extracting the 3D features. These sonar images contain noise which is undesired information that contaminates an image. In order to identify the objects present in the images received from the imaging sonar fitted onboard an AUV, a process called segmentation is employed. The segmentation methods include Edge detection, Canny Edge detection, Adaptive Thresholding, Fuzzy C means Thresholding and Adaptive Histogram Equalization. Even after segmentation of the real-time sonar images, images contain noise. So to further remove the noise from the sonar images and to identify the objects clearly, a new Image synthesis algorithm is developed. The proposed algorithm combines substantial information from several segmentation methods of original sonar images using mathematical techniques in order to create a single composite image. The resultant comprehensive image retains all the important features of the individual images. In order to get the complete 3D information of the object i.e., to know the depth information, the 2D images of the object are taken at different elevation angles of the sonar and are used to reconstruct the 3D shape of the object. From the available data, in order to reconstruct the 3D object a new surface construction algorithm is developed. The algorithm consists of (i) acquiring data points on the surface of the solid using sonar, (ii) reconstructing the surface from these points. The developed algorithms are validated with the real time data.

2. Sonar Operating Principle

Sonar refers to the application of sound for the detection and location of underwater objects. Sonar is the most successful method used for detecting the presence of objects underwater. The simplest sonar devices send out a sound pulse from a transducer and then precisely measure the time it takes for the sound pulses to reflect back to the transducer. The distance to an object can be calculated using this time difference and the speed of sound in the medium. This principle of operation of the sonar is shown in Fig. 1.

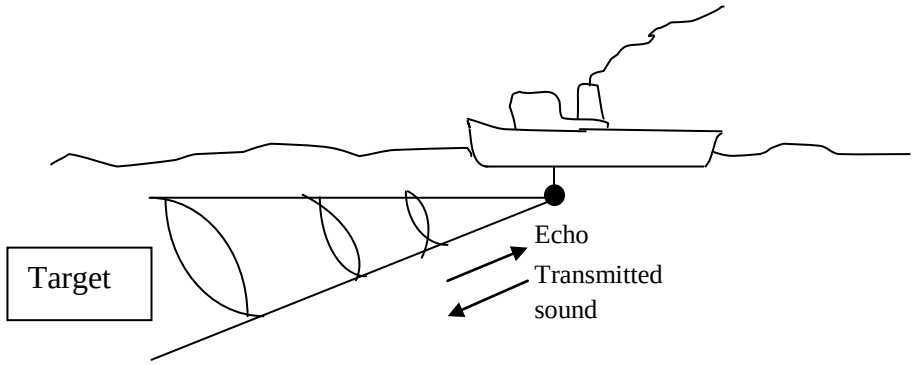

Fig. 1 Principle of operation of sonar

There are two types of the sonar: passive sonar and active sonar.

Passive Sonar

Passive sonar is a listening device; the sound waves produced by another source such as ships, biological creatures or due to seismic activities are received by the sonar's receiver and changed into electrical signals for analysis and also for display on a monitor. Since the frequencies emitted by the various sources are different, it is sufficient to receive these frequencies in order to identify the source. The direction of the source can also be found out either by beam forming method or through the triangulation method by having the measurements at different places. This will not be dealt here in detail as the aim of the research is related to the imaging sonars which are active.

Active Sonar

Active sonar is the one which sends the signals and receives the echo. Active sonar uses a transducer which converts electrical signal to sound waves. These sound waves are reflected back from the target and detected by the sonar's receiver as an echo. The receiver passes sound waves to the transducer which converts the sound back to electrical signals. Since the speed of the sound in water is known, the range and the bearing of the target can be

determined. This method is also known as echo-ranging. The block diagram of active sonar is shown in Fig. 2.

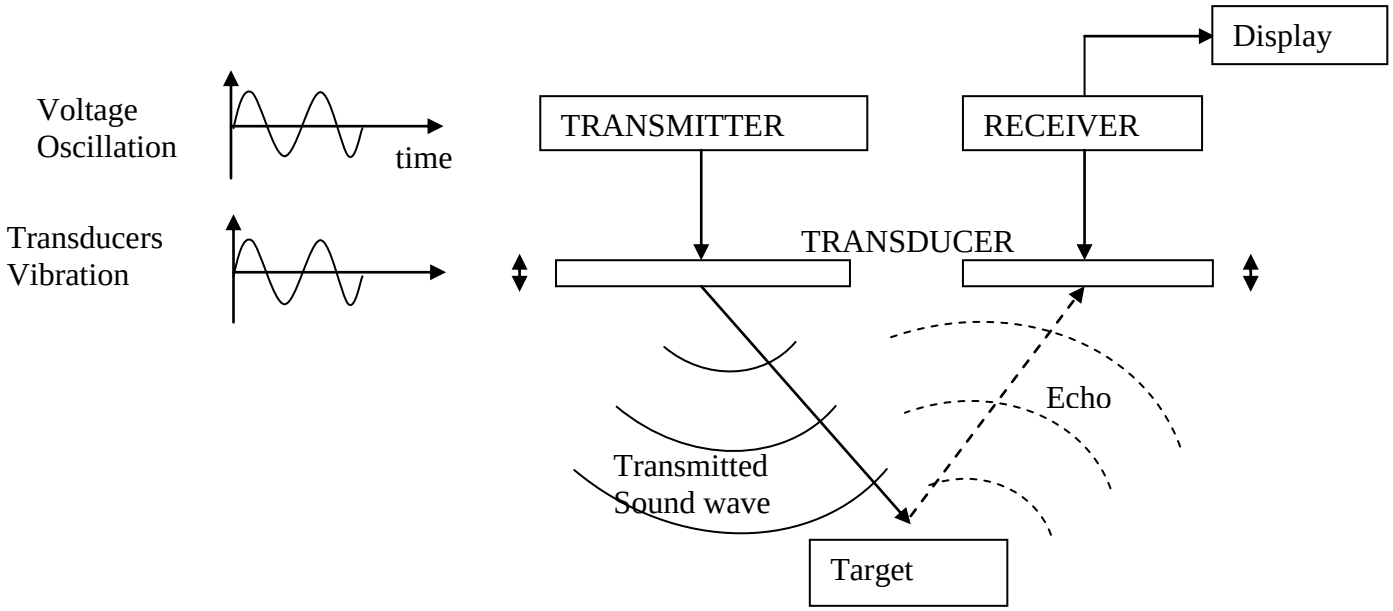

Fig. 2 Block diagram of active sonar

2.1 Sound Propagation in Underwater Medium

The basic theory of acoustics involves the study of vibration, waves and their propagation. If the direction of particle vibration is the same as the direction of wave propagation, then the wave is called a longitudinal wave. If the direction of particle vibration is perpendicular to the direction of wave propagation, then the wave is called a transversal wave. When a sound wave propagates in sea water, the structure of the water medium is changed, resulting in the spread of sound energy. The sensing of an underwater receiver for sound pressure is based on this sound pressure change. In the wave propagation process, particles in the sea water do not move from one place to another, but only vibrate around some fixed point. The acceleration speed of a particle is always proportional to the distance from a fixed point. This kind of motion is called resonance motion. It is the simplest form of periodic motion (Qihu Li., 2012). The expression of a one-dimensional differential equation of resonance motion is

$$\frac{d^2x}{dt^2} + w^2x = 0 \tag{1}$$

The solution of this equation is

$$x(t) = A\sin(\omega t) + B\cos(\omega t) \tag{2}$$

Where *A*, *B* are arbitrary constants and $\omega=2\pi f$ is the cycle frequency with unit rad/s, and the unit of *f* is Hz.

2.1.1 Velocity of sound wave

Sound travels more slowly in fresh water than in sea water. The speed of sound is determined by the water's bulk modulus and mass density. The bulk modulus is affected by temperature, dissolved impurities (usually salinity), and pressure. The density effect is small. The speed of sound (in feet per second) is approximately:

4388 + (11.25 × temperature (in °F)) + (0.0182 × depth (in feet)) + salinity (in parts-per-thousand)

This empirically derived approximation equation is reasonably accurate for normal temperatures, concentrations of salinity and the range of most ocean depths. Ocean temperature varies with depth, but at between 30 and 100 meters there is often a marked change, called the thermocline, dividing the warmer surface water from the cold, still waters that make up the rest of the ocean. The sonar may not produce the desired result as the sound originating on one side of the thermocline tends to be bent, or refracted, through the thermocline. The thermocline may be present in shallower coastal waters. However, wave action will often mix the water column and eliminate the thermocline. Water pressure also affects sound propagation: higher pressure increases the sound speed, which causes the sound waves to refract away from the area of higher sound speed. The mathematical model of refraction is called Snell's law.

The propagation velocity c of sound in the sea can be derived from the following adiabatic equation

$$c=\left(\frac{\partial p}{\partial \rho}\right)=\frac{1}{\rho K_a} \qquad (3)$$

where, *p* is the sound pressure, ρ is the density of water, and K_a is the adiabatic compression coefficient. In sea water, since pK_a is a function of temperature, salinity and pressure, the sound speed in sea water is also a function of temperature, salinity and pressure, but temperature is the dominant factor. In fresh water, the empirical formula for calculating sound speed is generally

$$c=1410+4.21t-0.037t^2+0.018d \text{ (m/s)} \qquad (4)$$

where, *t* is the temperature of sea water in ^0C; *d* is the depth (m). c ≈1,500 m/s, for $t = 20^0$C. The empirical formula for calculating sound speed in sea water is given by

$$c=1410+4.21t-0.037t^2+1.1S+0.018d \text{(m/s)} \qquad (5)$$

where S is the salinity (%). C ≈1,500 m/ s when t = 14°C, S = 34.5, d = 15m.

Because the propagation characteristics of sound in the sea strongly depend on the sound speed, it is very important to understand the distribution of sound speed for any specific area. The relation between sound speed and depth is called the sound speed profile (SSP). The SSP is related to the latitude, season, and day /night.

2.1.2 Sound pressure and sound power

"Sound power" and "Sound pressure" are two distinct and commonly confused characteristics of sound. Sound power or **acoustic power** is a measure of the total sound power emitted by a source in all directions in watts (joules per second) per unit time *t*. Sound power levels are connected to the sound source and are independent of distance. Sound power levels are indicated in decibel as follows

$$L_w = 10\log_{10}\frac{I}{I_o} \tag{6}$$

where sound power I_o is chosen to be a reference sound power, define it as 0 dB, and then any other sound power I has the dB value of $20\log I/I_o$ dB with respect to reference level.

Sound pressure is a pressure disturbance in the air whose intensity is influenced not only by the strength of the source, but also by the surroundings and the distance from the source to the receiver and diminishes as a result of intervening obstacles and barriers, air absorption, wind and other factors. Sound pressure levels quantify in decibels and the intensity of given sound sources are indicated in decibels.

Sound pressure level (SPL) $L_p = 10\log_{10}\frac{P}{P_o}$ (7)

Where sound pressure P_o is chosen to be a reference sound pressure, define it as 0 dB, and then any other sound pressure P has the dB value of $20\log P/Po$ dB.

A frequently used method of estimating the sound power level at a source $L_w$is to measure the sound pressure level L_p at some distance r, and solve for L_w. If the source is in free space

$$L_w = L_p - 10\log_{10}\left(\frac{1}{4\pi r^2}\right) \tag{8}$$

or if the source is on the floor or on a wall, such that it radiates into a half sphere.

$$L_w = L_p - 10\log_{10}\left(\frac{2}{4\pi r^2}\right) \tag{9}$$

2.1.3 Transmission loss of sound in underwater

Transmission Loss is the parameter that compares the amount of intensity of the signal at a specific range from the source to the source intensity at one yard. The equation for this would be:

$$TL = 10\log\frac{I(1yd)}{I(r)} \tag{10}$$

In sonar equations, transmission loss *TL* is an important parameter in sonar design because the performance of a sonar system depends only on the transmission loss. When a sound wave propagates in an ocean environment, the sound intensity will gradually decrease with travel distance, because of the following reasons:

i) The geometrical spread of the wave front, spherical or cylindrical spreading,

ii) The loss of the sound wave at the sea surface and the sea floor,

iii) Sound absorption,

iv) Sound reflection.

Spreading and Cylindrical Losses

Sound waves while propagating underwater they get attenuated due to cylindrical and spherical spreading of the energy. Cylindrical spreading presents underwater only when the sea surface and the sea floor are flat. However spherical spreading presents underwater in all kinds of sea environment. The transmission loss increases linearly in both spherical and cylindrical spreading and the transmission loss due to spherical spreading is twice the transmission loss due to cylindrical spreading.

2.1.3.1 Spreading Loss

Let's assume a point source which emits a signal in all directions (that is in three dimensions). The source would produce wave fronts that were spheres that would grow in size as the wave propagates away from the source as shown in Fig 3.

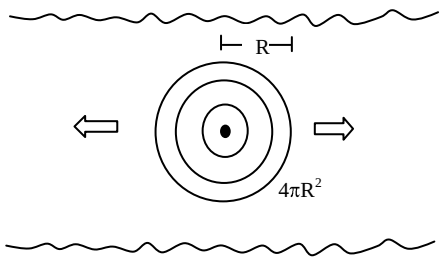

Fig. 3 Spherical spread

$$TL = 20\log r \tag{11}$$

The above equation is for transmission loss only due to spherical spreading. In this case, from 1 m to 100 m, the intensity of the sound wave will attenuate by 40 dB. Spherical spreading is the most dominant factor in the transmission loss portion of the passive sonar equation. As the range increases the transmission loss increases linearly as shown in Fig 4 and the corresponding values are given in Table 1.

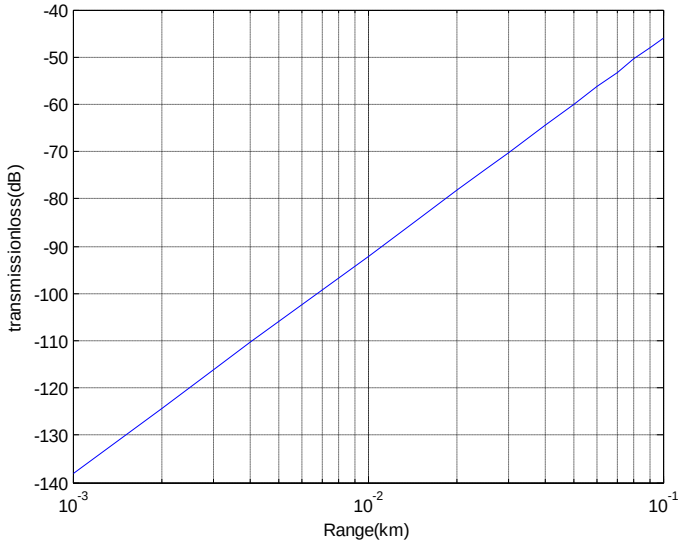

Fig. 1 Typical transmission loss curve of band limited signal

Range(m)	Transmission loss(dB)
1	-138.1
5	-105.9
10	-92.1
20	-78.2
50	-59.9
70	-53.1
100	-46.0

Table 1 Range prediction by calculation of transmission loss for spherical spread

2.1.3.2 Cylindrical Spreading

In the propagation of a sound wave, if the sea surface and sea floor are relatively flat, sound reflection and absorption are negligible, so the spread of a sound wave can be considered as cylindrical (Fig. 5). The transmission loss is proportional to the distance *R*. As the range increases the transmission loss increases linearly as shown in Fig 6 and the corresponding values are given in Table 2.

The transmission loss due to cylindrical spreading is half of the spherical spreading.

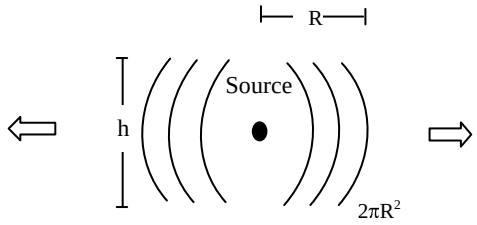

Fig. 5 Cylindrical spread

$$TL(R) = 10\log R \qquad (12)$$

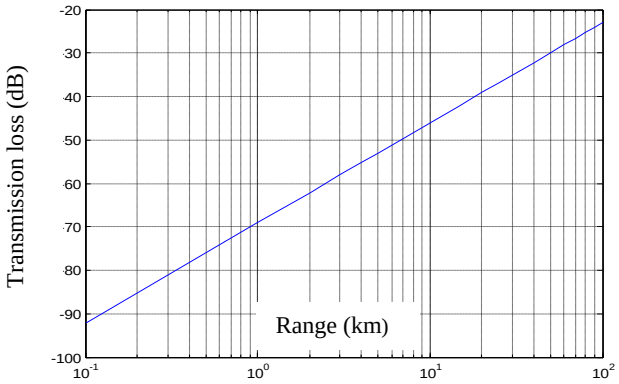

Fig.6 Typical transmission loss curve of band limited signal

Range(m)	Transmission loss(dB)
1	-69.0
5	-52.9
10	-46.0
20	-39.1
50	-29.9
70	-26.5
100	-23.0

Table 2 Range prediction by calculation of transmission loss for cylindrical spread

The only limitation of this equation is that it does not take into account the spreading of the wave spherically until it reaches the "transition range" where the wave starts to spread cylindrically.

2.1.4 Sound absorption in underwater

Sound absorption in sea water is one of the important characteristics of an acoustic channel. This is because, as the information carrier, in the propagation of a sound wave, energy dissipation is the main characteristic of a channel. Sea water is not an ideal medium

for sound transmission. The absorption of sound in seawater forms part of the total transmission loss of sound from a source to a receiver. It depends on the seawater properties, such as temperature, salinity and acidity as well as the frequency of the sound. Absorption is the conversion of acoustic energy to heat in the fluid. There are three main causes of absorption losses:

i. Viscosity

ii. Change in molecular structure

iii. Heat conduction

Attenuation losses in sea water occur from both sound absorption losses and scattering losses. This attenuation causes a decrease in the amplitude of the wave and an exponential decrease in the acoustics pressure resulting in more spreading loss. To account for attenuation in the transmission loss equation, a new term, α must be defined, the attenuation coefficient. Using this new term, the transmission loss can be calculated using the equation:

$$TL_{attenuation} = \alpha(r - (1yd)) \times 10^{-3}\, dB \qquad (13)$$

where r is in yards. Generally, since the range, r, is usually much greater than 1 yard, we can ignore the -1yard term in the equation. Thus the transmission loss can be expressed as:

$$TL_{attenuation} = \alpha(r \times 10^{-3}) dB \qquad (14)$$

The most difficult problem in the transmission loss is to determine a correct value for α, i.e., the attenuation coefficient and the various factors that affect the attenuation coefficient are given below.

i) Viscosity

The viscosity losses are due to two distinct effects. Each of these effects is dependent on not only how the molecules act together in the medium as defined by the coefficients of both shear and volume viscosity but also the frequency of the sound waves.

When both terms are combined and nominal values used for the density, speed of sound and the coefficients, the value for the attenuation coefficient becomes

$$\alpha = 2.75 \times 10^{-4}\, f^2 \qquad (15)$$

where f is the sound wave frequency in kHz.

ii) Ionic Relaxation

The below equation describes how Ionic Relaxation affects the attenuation coefficient is

$$\alpha_{MgSO4} = \frac{40 f}{4100 + f^2} \qquad (16)$$

where frequency, f, is in kHz.

Though many factors affect this complex process, simply suffice it to say that an equation for this process' affect on α would be

$$\alpha_{boron\text{-}borate} = \frac{0.1 f^2}{1+ f^2} \tag{17}$$

iii) A non-absorption factor, scattering

The last factor that contributes to losses is the scattering of sound energy due to in homogeneities in seawater. This factor can be approximate as a constant, not dependant on frequency and would only be a dominant factor below 100 Hz or so. This can be expressed as

$$\alpha_{scattering} = 0.003 dB / kyd \tag{18}$$

When all these factors are combined, the equation for transmission loss then becomes:

$$TL = \alpha (r \times 10^{-3}) dB \tag{19}$$

where

$$\alpha = \left(0.003 + \frac{0.1 f^2}{1+ f^2} + \frac{40 f^2}{4100 + f^2} + 2.75 \times 10^{-4} f^2 \right) \text{dB/kyd} \tag{20}$$

The unit dB / ky can be converted to dB / km by multiplying with a factor of 1.094 then absorption coefficient can be written as

$$\alpha = 1.094 \times \alpha_0 (dB / km) \tag{21}$$

The characteristics of absorption of sound in water is shown in Fig. 7 and corresponding values are given in Table 3

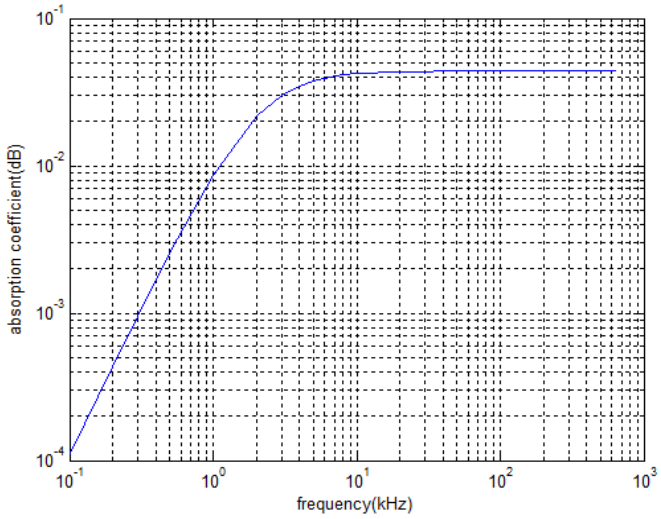

Fig. 7 Absorption of sound in sea water

Frequency(kHz)	Absorption coefficient(dB)
0.1	1.1114e-004
0.5	0.0025
1.0	0.0086
2.0	0.0217
3.0	0.0302
4.0	0.0349

Table 3 Variation of absorption coefficient with frequency

3. Determination of Range Resolution of Monotonic and Chirp technology Sonar

Monotonic Sonar

In monotonic sonars, the transmitted acoustic pulse consists of an on/off switch modulating the amplitude of a single carrier frequency. Fig. 8 below shows how this relationship exists between the transmitted signal and the output produced by the receiver circuitry in the sonar. It can be seen that the receiver does not decode each cycle of the transmitted pulse, but instead produces the 'envelope' of its overall amplitude as shown in Fig. 8

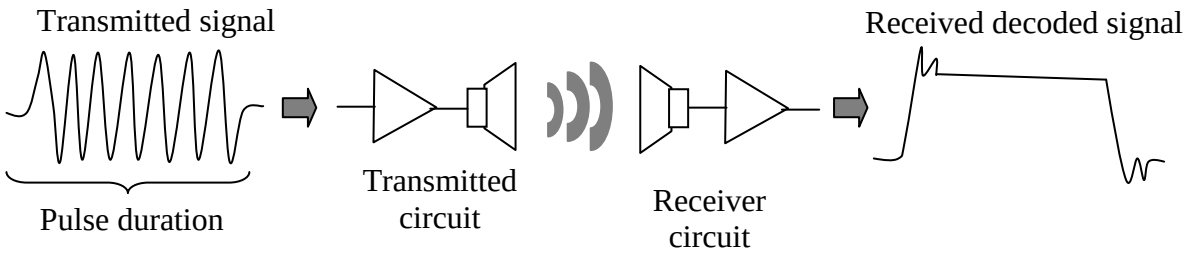

Fig. 8 Monotonic sonar acoustic signals

The ability of monotonic acoustic systems to resolve targets is better if the pulse duration is short; this, however, has its drawbacks. Ideally, long transmit pulses are needed to pump enough acoustic energy into the water for good identification of the long range targets, but due to the velocity of sound (VOS) through water (typically around 1500 metres / second), each pulse occupies an equivalent 'distance' related to its duration - this is referred to as 'range resolution', and is given by the following equation.

$$\text{range resolution} = \frac{\text{pulse length} \times \text{speed of sound}}{2} \tag{22}$$

The duration of the de-chirped pulse equals the inverse of the bandwidth.

$$\text{pulse length} = \frac{1}{\text{bandwidth}} \tag{23}$$

For example, if the smallest pulse duration is 50 microseconds, and combining this with the typical VOS of 1500 metres / second, a range resolution of 27.5mm is obtained.

The 'range resolution' effectively determines the ability of the sonar to distinguish two close by targets; therefore using the above example, if two targets are less than 27.5mm apart then they cannot be distinguished from each other. The range resolutions for different pulse durations is shown in Table 4 and its performance is shown in Fig. 10. The net effect is that the system will display a single large 'combined' target, rather than multiple smaller targets as shown in Fig. 9.

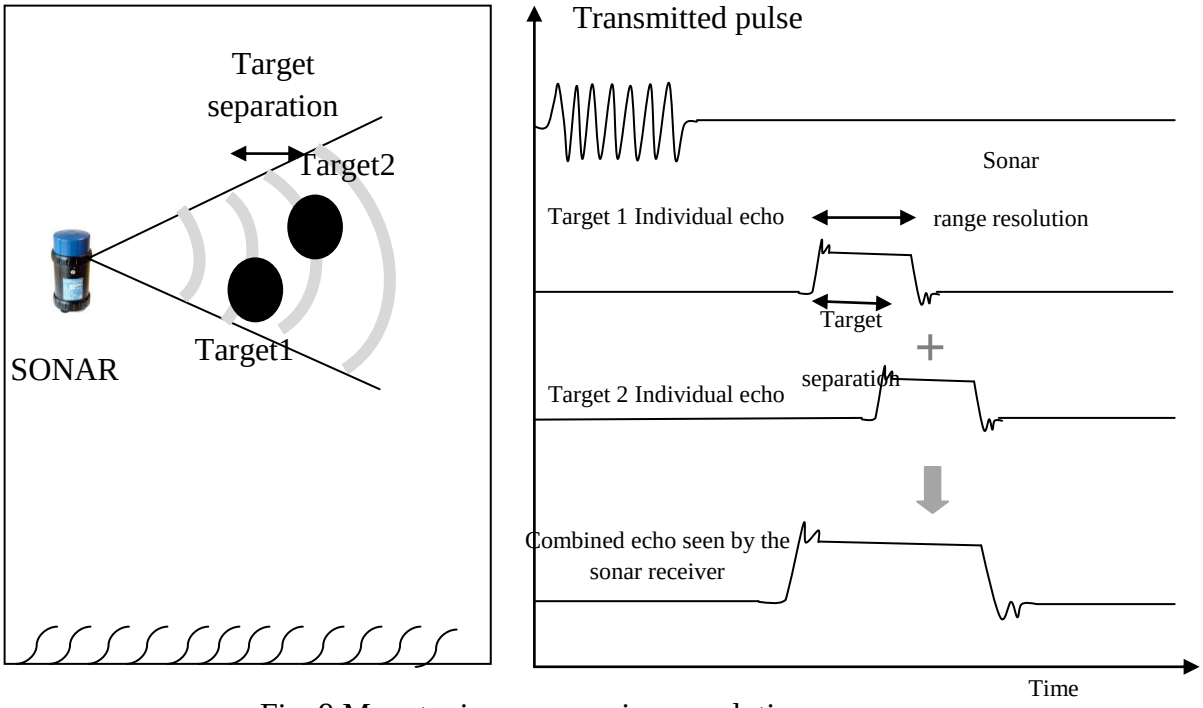

Fig. 9 Monotonic sonar receiver resolution

Frequency used (kHz)	Pulse Duration (micro seconds)	Sound velocity (m/s)	Range Resolution (mm)
25	50	1500	27.5
25	100	1500	75
25	150	1500	112.5
25	200	1500	150
25	250	1500	187.5
25	200	1500	225
25	250	1500	262.5
25	400	1500	200
25	450	1500	227.5
25	500	1500	275

Table 4 Range resolutions for different pulse durations of conventional sonar

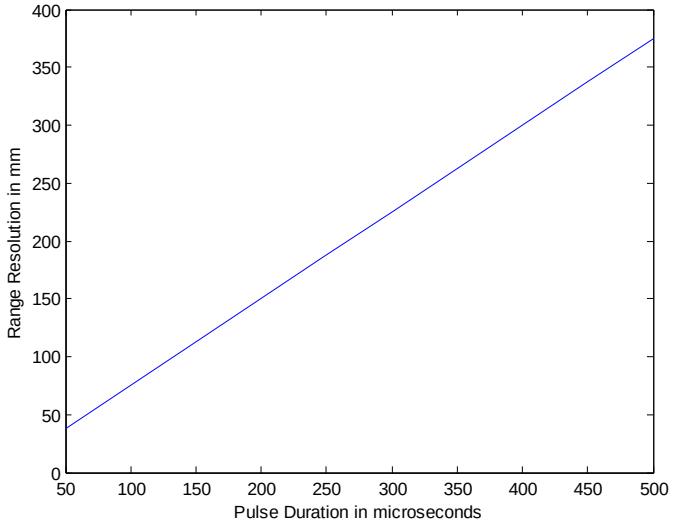

Fig. 10 Variation of range resolution for various pulse durations for fixed frequency sonar

Chirp Technology Sonar

Instead of using a pulse of a single carrier frequency, in the chirp technology sonar the frequency within the pulse is changed (swept) throughout the duration of transmission, from one frequency to another. For example, at the start of the transmission the sonar may operate at 200KHz, and at the end, it may have reached 250KHz. The difference between the starting and ending frequency is known as the 'bandwidth' of the transmission, and typically the centre frequency of the transmission is used to identify the sonar (in this case it would be a 225KHz sonar). By constantly changing its frequency over time, this 'chirped' transmission can be thought of as having a unique acoustic signature, and so if two pulses now overlap (as the targets are closer than the range resolution), the known 'frequency versus time' information can be used to separate them apart.

With new high-speed Digital Sonar Technology (DST) signal processing techniques, the sonar receiver contains a 'pattern-matching' circuit that looks for its transmitted 'chirp' being echoed back from targets, and its receiver now produces a sharp 'spike' when a good match is found (whereas the monotonic sonar produces an output having the same duration as its transmit pulse) as shown in Fig. 11.

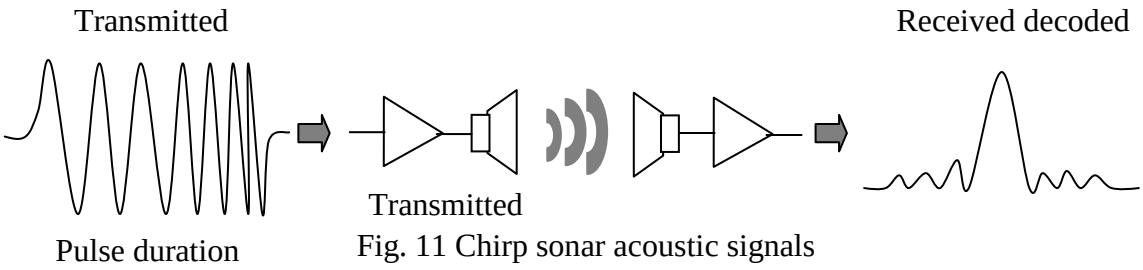

Fig. 11 Chirp sonar acoustic signals

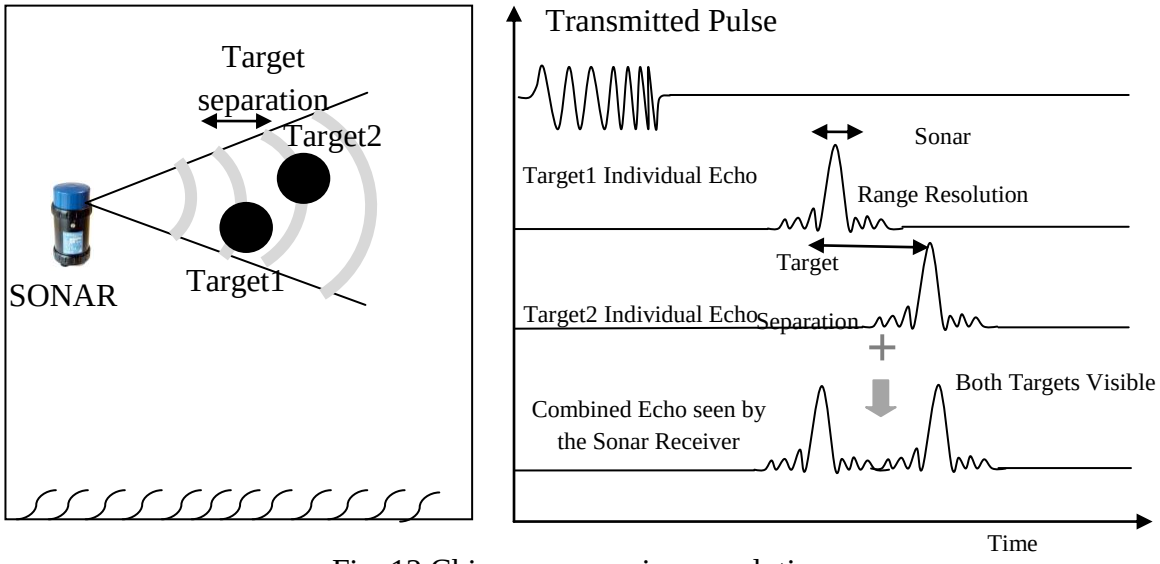

Fig. 12 Chirp sonar receiver resolution

In all sonar systems, higher frequency content is invariably associated with an increase in resolution and a decrease in penetration. Chirp technology, as implemented in our chirp systems, reduces the trade-off between signal range and image resolution. Chirp sonar receiver resolution is shown in Fig. 12. The range resolution of chirp technology sonar is given as

Range resolution = (velocity of sound) / (bandwidth x 2) (24)

The bandwidth of a typical chirp system is 100 kHz, and using the typical VOS of 1500 metres / second, the range resolution obtained is 7.5mm which is better than conventional sonar. The range resolutions for different bandwidths are shown in Table 5 and its performance is shown in Fig. 13.

Bandwidth (kHz)	Velocity of sound (m/s)	Range Resolution (mm)
100	1500	7.5
150	1500	5
200	1500	2.75
250	1500	2
200	1500	2.5
250	1500	2.142
400	1500	1.875
450	1500	1.666
500	1500	1.5
550	1500	1.262

Table 5 Range resolutions for different bandwidths of chirp technology sonar

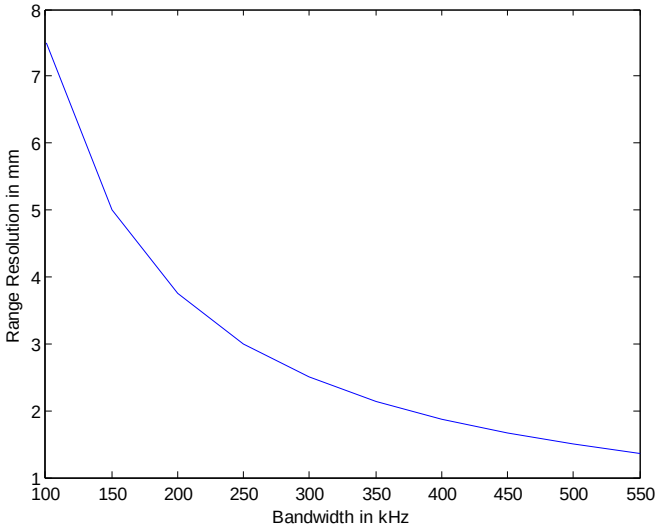

Fig. 13 Variation of range resolution for various bandwidths for chirp technology

The resolution of an imaging system is measured by its ability to separate closely spaced objects. In other words, to detect discrete echoes returning from the interfaces between layers or targets on the seafloor. The vertical resolution of an acoustic sub-bottom profiler refers to the minimum distance that can be visually distinguished in the image produced by the system. A sonar system with a 10 cm resolution will resolve layers that are atleast 10 cm apart. In a conventional single-frequency system, the limit of resolution is determined by the pulse width of the transmitted waveform. In a multi-frequency system, it is the bandwidth of the transmitted pulse that sets the system's theoretical resolution. The theoretical sonar range resolution, either cross-track in the case of side scan sonar or vertical in the case of a sub-bottom profiling, is calculated by multiplying the length of the compressed pulse by the speed of sound, and dividing the product by two to account for the ping's round trip travel time.

4. Chirp technologies used in Sonar

There are two types of chirp technologies in use today depending on the application. They are i) Linear chirp and ii) Exponential chirp

Linear Chirp

In a *linear* chirp, the instantaneous frequency $f(t)$ varies linearly with time as shown in Fig. 14

$$f(t) = f_0 + kt \tag{25}$$

where f_0 is the starting frequency (at time $t = 0$), and k is the rate of frequency increase or chirp rate. The corresponding time-domain function for a sinusoidal linear chirp is given by

$$x(t) = \sin\left[2\pi \int_0^t f(t)\,dt\right] \tag{26}$$

$$= \sin\left[2\pi \int_0^t (f_0 + kt)\,dt\right]$$

$$x(t) = \sin\left[2\pi\left(f_0 + \frac{k}{2}t\right)t\right] \tag{27}$$

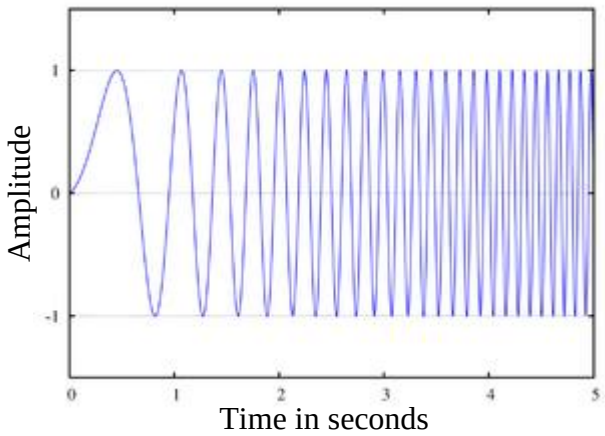

Fig. 14 A linear chirp waveform

In the frequency domain, the instantaneous frequency described by the equation $f(t) = f_0 + kt$ is accompanied by additional frequencies (harmonics) which exist as a fundamental consequence of frequency modulation. These harmonics are quantifiably described through the use of Bessel Functions. However with the aid of Frequency vs. Time profile Spectrogram, one can readily see that the linear chirp has spectral components at harmonics of the fundamental chirp.

Exponential Chirp

In a geometric chirp, also known as an exponential chirp as shown in Fig. 15, the frequency of the signal varies with a geometric relationship over time. In other words, if two points in the waveform are chosen, i.e. t_1 and t_2, and the time interval between them $t_2 - t_1$ is kept constant, the frequency ratio $f(t_2)/f(t_1)$ will remains constant.

In an *exponential* chirp, the frequency of the signal varies exponentially as a function of time

$$f(t) = f_0 k^t \tag{28}$$

where f_0 is the starting frequency (at $t = 0$), and k is the rate of exponential increase in frequency. Unlike the linear chirp, which has a constant chirp rate, an exponential chirp has an exponentially increasing chirp rate. The corresponding time-domain function for a sinusoidal exponential chirp is given by

$$\begin{aligned} x(t) &= \sin\left[2\pi \int_0^t f(t)\,dt\right] \\ &= \sin\left[2\pi f_0 \int_0^t k^t dt\right] \\ x(t) &= \sin\left[2\pi f_0 \frac{k^t - 1}{\ln(k)}\right] \end{aligned} \tag{29}$$

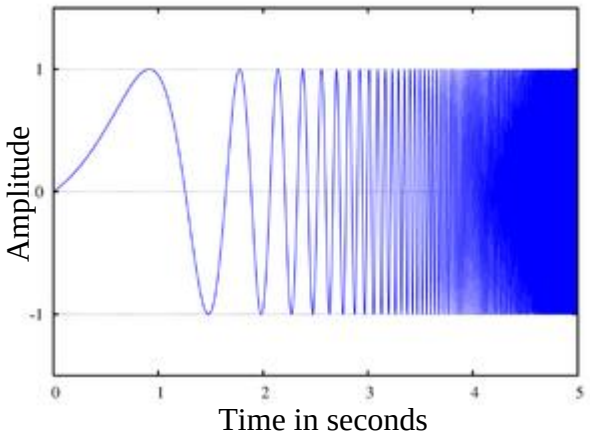

Fig.15 An exponential chirp waveform

As in the case for a linear chirp, the instantaneous frequency of the exponential chirp consists of the fundamental frequency $f(t) = f_0 k^t$ accompanied by additional harmonics.

A geometric chirp does not suffer from reduction in correlation gain if the echo is Doppler-shifted by a moving target. This is because the Doppler shift actually *scales* the frequencies of a wave by a multiplier (shown below as the constant c).

$$f(t)_{\text{Doppler}} = cf(t)_{\text{Original}} \tag{30}$$

From the above equations, it can be seen that this actually changes the rate of frequency increase of a linear chirp (*kt* multiplied by a constant) so that the correlation of the original function with the reflected function is low.

Because of the geometric relationship, the Doppler shifted geometric chirp will effectively start at a different frequency, f_0 multiplied by a constant, but follow the same pattern of exponentially increased frequency. For instance, the end of the original wave, will still overlap perfectly with the beginning of the reflected wave and the magnitude of the correlation will be high for that section of the wave.

A chirp signal can be generated with analog circuitry via a voltage controlled oscillator (VCO) and a linearly or exponentially ramping control voltage. It can also be generated digitally by a digital signal processor (DSP) and a digital to analog convertor (DAC) by varying the phase angle coefficient in the sinusoid generating function.

5. Pulse Compression Method for Chirp technology Sonar

Pulse compression is a signal processing technique mainly used in radar and sonar to increase the range resolution as well as the signal to noise ratio (SNR). This is achieved by modulating the transmitted pulse and then correlating the received signal with the transmitted pulse. It involves the transmission of a long coded pulse and the processing of the received echo to obtain a relatively narrow pulse. The transmitted long pulse may be generated from a narrow pulse. A narrow pulse contains a large number of frequency components with a precise phase relationship between them. If the relative phases are changed by a phase-distorting filter, the frequency components combine to produce a stretched or expanded pulse. This expanded pulse is the pulse that is transmitted. The received echo is processed in the receiver by a compression filter. The compression filter readjusts the relative phases of the frequency components so that a narrow or compressed pulse is again produced. The pulse compression ratio is the ratio of the width of the expanded pulse to that of the compressed pulse. The pulse compression ratio is also equal to the product of the time duration and the spectral bandwidth (time bandwidth product) of the transmitted signal.

The ‘received signal’ is the baseband signal recorded by the sonar after it has been demodulated. The received signal will contain overlapping waveforms at different magnitudes which have been reflected from the different scattering points of the target. If the reflection is from a single point target it will have the same form as the transmitted waveform although it will be distorted by the sonar system. This received signal will then be

compressed to form a single impulse. The data samples are the values of the received signal recorded by the sonar using the analog to digital converters. These are complex values recorded in pairs from the in-phase and quadrature phase demodulators. The pulse compressed received signal is the ‘range profile’ of the target which consists a series of ‘cells’ where each cell has the width of an ideal pulse i.e., the limit of the resolution. This means that the number of cells in the range profile is equal to the number of data samples in the received signal except that the ends of the signal cannot be compressed as they may only contain part of a reflected waveform. It is the range profile that is required to carry out further processing.

Pulse compression is the method used to calculate the range profile, if the received signal and the transmitted waveforms are given. This can be done by either of the following two methods:

1. Deconvolution – Reversing the convolution of the range profile with the transmitted waveform. This must be done in the frequency domain.
2. Correlation – ‘Searching’ for the waveform in the received signal. The range profile is equal to the correlation of the complex transmitted waveform and the complex received signal, with a range shift. This is because the received signal contains copies of the transmitted signal all added together, one for each pulse in the range profile. A time reversed and conjugated copy of the transmitted waveform is convolved with the received signal to produce the correlation. Unfortunately deconvolution is less robust than correlation, hence by default correlation is preferred.

Block diagram of Pulse Compression Sonar

In pulse compression technique, the transmitted signal is either frequency modulated or phase modulated and the received signal is processed using a specific filter called "matched filter". In this form of pulse compression, a long pulse of duration, T is divided into N sub pulses each of width, τ.

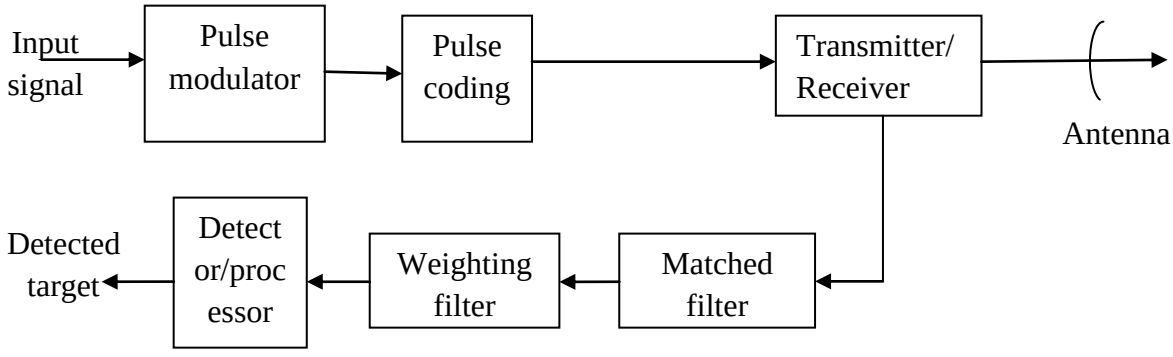

Fig. 16 Block diagram of pulse compression sonar

The block diagram shows the pulse modulator responsible for generating the continuous-modulated pulse and the next stage i.e. pulse coding technique generates frequency modulated pulse or chirp pulse (Fig. 16). In addition to generating the transmitted pulse, the frequency modulator or phase coding technique also plays a role in the design of the pulse compression filter. The pulse-compression filter is an example of a matched filter because the filter is specially designed to recognise the characteristics of the transmitted pulse as they are returned to the receiver in the form of reflected pulses. To that extent , the filter is been matched to the transmitted waveform. The received pulses with similar characteristics to the transmitted pulse are recognised by the matched filter where other received signals pass relatively unnoticed by the receiver.

6. Matched filter response for modulated signal

The above results can also be extended to find the matched filter response when $s\ t$ is a linear frequency modulated (LFM) pulse or chirp pulse. The pulse-compression filter or matched filter simply performs a strong correlation between what was transmitted i.e, LFM pulse or chirp pulse and what was received. The effects of this form of processing on two pulses with the same duration are shown in the following Fig. 17. In the continuous frequency (CF) example, the matched filter (correlation) response shows the triangular envelope as shown in Fig. 17 (a). However, in the chirp example with the same duration, the matching pulse-compression filter generates an interesting pulse called a sinc pulse with a much narrower peak, and hence a superior range resolution as shown in Fig. 17 (b).

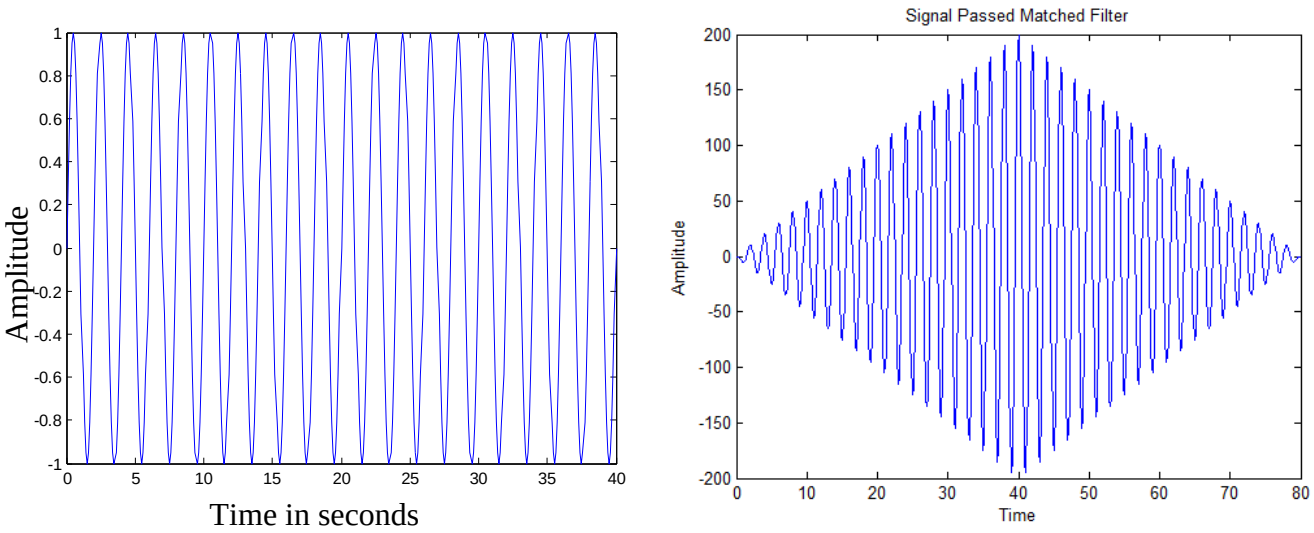

Fig. 17 a) Response of matched filter for a continuous frequency signal

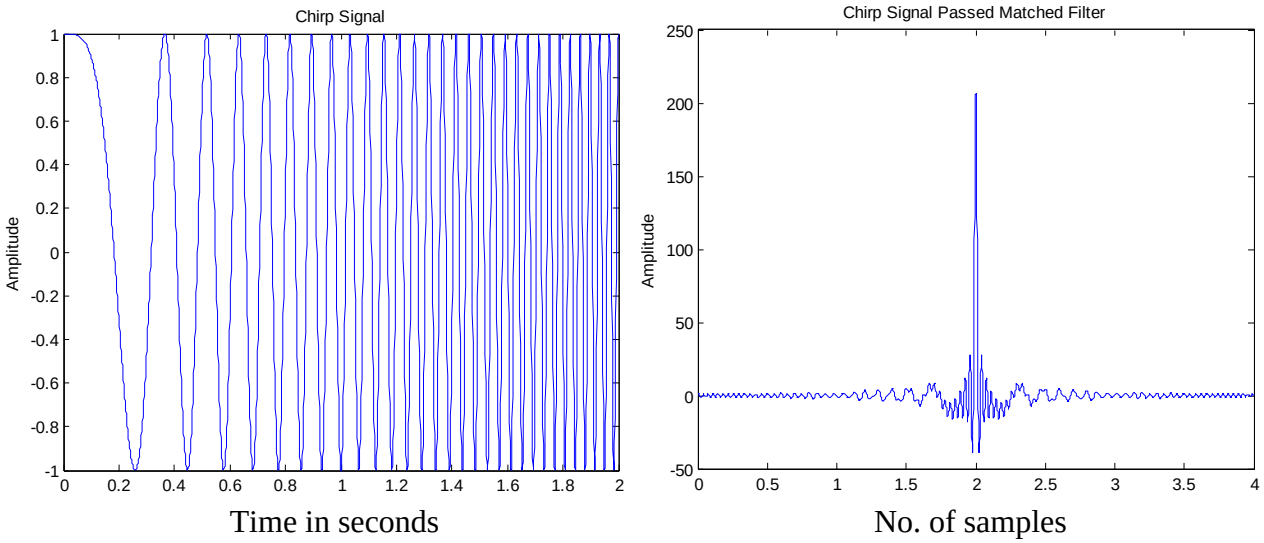

Fig. 17 b) Response of matched filter for a chirp signal

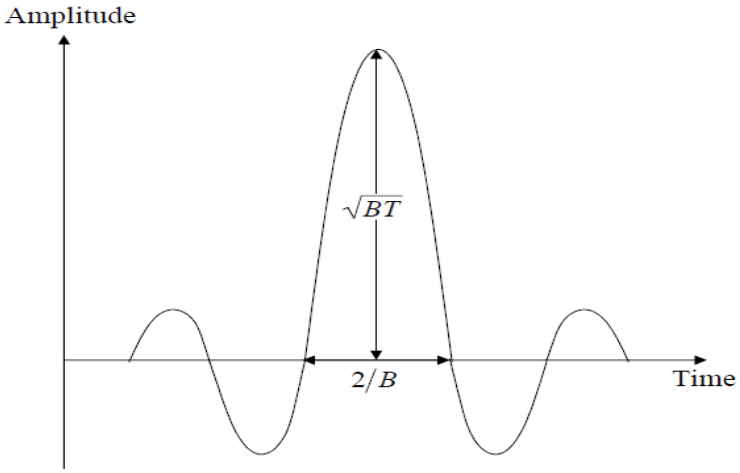

Fig. 18 Typical output from a pulse compression filter

From Fig. 18, it is observed that the width of the sinc pulse is inversely proportional to the bandwidth of the uncompressed pulse and the height is proportional to the product of the bandwidth and uncompressed pulse width.

The output of the pulse-compression filter forms the input to the detector section of the pulse-compression sonar. It is therefore desirable to have a very narrow and tall pulse (just as it is in a standard pulse sonar system). The main points to note from Fig. 18 are that the input to the filter is a relatively broad and low power pulse. The output pulse, however, is very narrow and strong. These are the two very desirable characteristics from pulse sonar.

When looking at the output of the pulse-compression filter as shown in Fig 17, the sidelobes on either side of the central pulse are reasonably large. These sidelobes are called range

sidelobes. The range sidelobes are a direct consequence of the pulse-compression filtering process. They are undesirable because they can lead to false alarms and range ambiguity.

The solution to the range sidelobe problem is to use a weighting factor in the pulse-compression filter or at transmitter side that effectively detunes or mismatches the filter and consequently attenuates the sidelobe levels. Unfortunately, the advantages of the pulse compression process are slightly reduced by this technique in which the compressed pulse will have reduced amplitude and an increased pulse width.

7. Investigation of suitable windowing technique for underwater object detection

A chirp signal has a time-varying frequency, and provides the right kind of spectral coverage. Chirping has some major advantages over continuous signals. If the same frequencies are transmitted at all time, one waveform will look like the other one. There is lots of information contents in the received signal however, one can't isolate time events producing that frequency content. If the chirps are reduced to short time intervals, the time resolution improves dramatically, though it is harder to distinguish the frequency content in the return signals. The abrupt edges of the squared pulse have some negative side effects. In the echo results, one can't tell which effects come from the signal and which come from the artificial edge discontinuity. To avoid these unresolvable problems, windowing techniques are employed.

Window functions are used to obtain a compromise between a narrow main lobe for high resolution and low side-lobes for low spectral leakage. High resolution provides accurate estimation of a target and can additionally separate two targets that are closely spaced in frequency. In the spatial domain it allows accurate estimation of two closely spaced scatterers. Low spectral leakage improves the detectability of a weak sinusoid in the presence of a strong sinusoid that is not been centered.

In practical cases windowing techniques are mostly used after matched filter section of pulse compression technique. After applying pulse compression to the received signal of the sonar, the response of the matched filter is shown in Fig. 19.

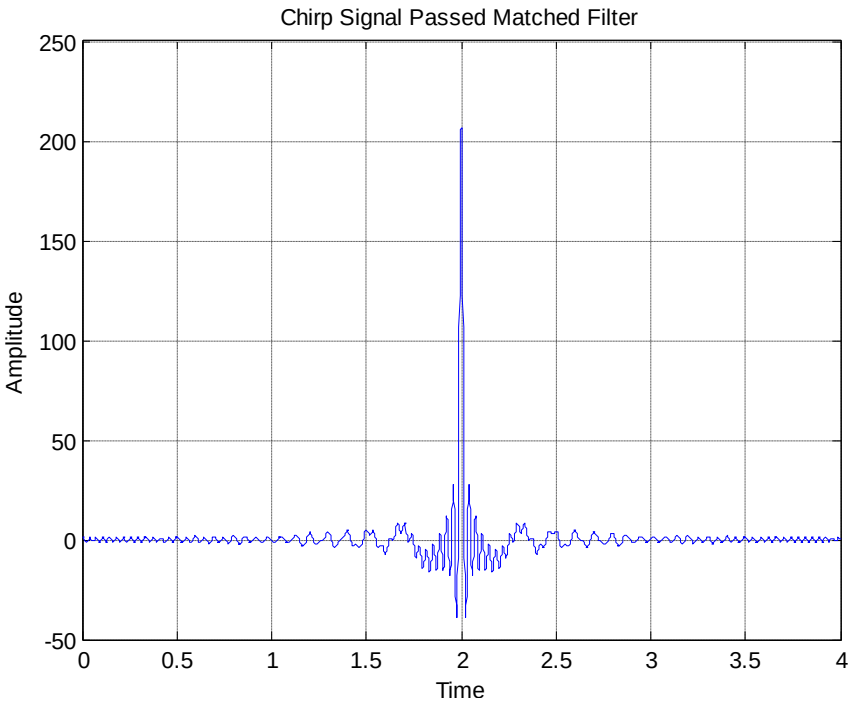

Fig. 19 Response of matched filter for received signal

Even after passing signal through the matched filter the noise still remains in the signal. So windowing technique is applied after the matched filter and the response of the signal is shown in below Fig. 20. So compared to the above Fig. 19 the noise is reduced to much extent.

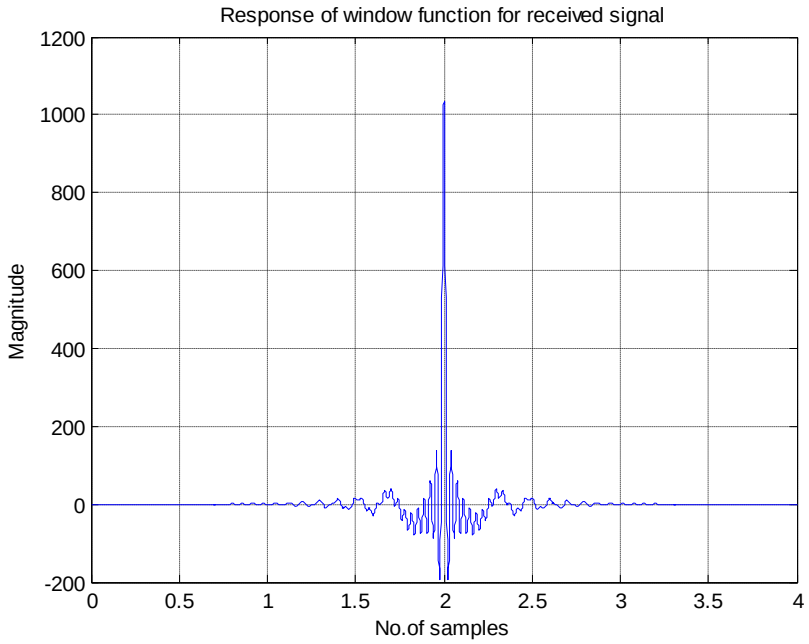

Fig. 19 Envelope of matched filter output passed through window

There are two common situations: detection of a spectral component in the presence of broadband noise; or distinguishing between narrow band spectral components. The choice of window function may be different in the two cases of detection or resolution. The choice of the window is important. It determines the trade-off of time versus frequency resolution which affects the smoothness of the spectrum and the detectability of the frequency peaks. The most commonly used windows are Rectangular, Triangular, Hamming, Hanning, Kaiser, Blackman Harris windows and many others. In the subsequent paragraphs, some of the windowing techniques are analyzed and compared.

7.1 Rectangular Window

The rectangular window is sometimes known as a Dirichlet window. It is the simplest window, taking a portion of the signal without any other modification leads to discontinuities at the endpoints.The rectangular window, is therefore rarely used for its low stopband attenuation. The first lobe has attenuation of 13dB and the narrowest transition region. Unlike other window functions which are designed based on the compromise between 'Narrow Transition' and 'Stopband Attenuation' this window is characterized by extreme values.

It is easy to find rectangular window coefficients as all coefficients between 0 and N-1 (N-filter order) are equal to 1, which can be expressed in the following way:

$$W[n] = 1;\ 0 \leq n \leq N-1 \qquad (31)$$

When applying this function to the received signal of pulse compression sonar, the magnitude response both in spatial and frequency domain is shown in Fig. 20(a) and (b).

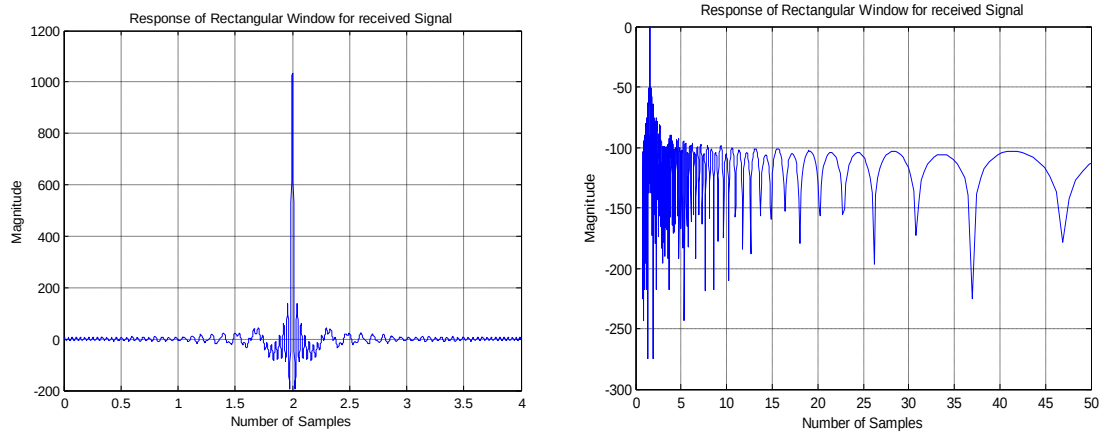

(a)Time domain (b) Frequency domain

Fig. 20 Magnitude response of received signal after rectangular window

7.2 Hann window

The Hann window is used to reduce effects on frequency characteristic produced by the final samples of a signal being filtered. This window has higher stop band attenuation than those designed with triangle function. The first side lobe in the frequency domain of this filter has 31dB attenuation.

The Hann window coefficients can be expressed as:

$$W[n]=\frac{1}{2}\left[1-\cos(\frac{2\pi n}{N-1})\right];0\le n\le N-1 \tag{32}$$

The magnitude response of received signal after passing through the Hann window is shown in Fig. 21.

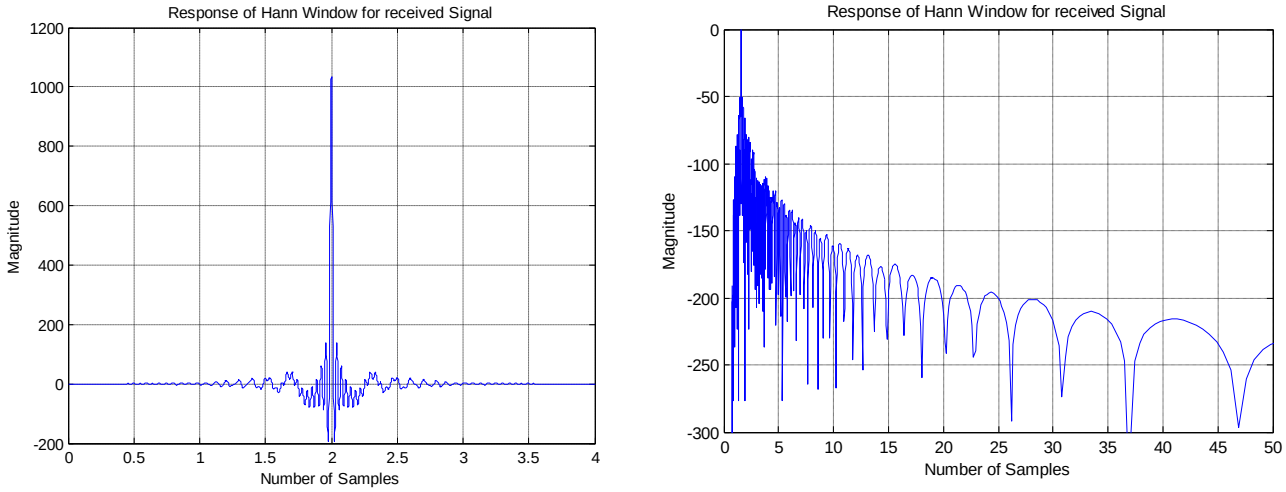

(a) Time domain (b) Frequency domain

Fig. 21 Magnitude response of received signal after hann window

7.3 Hamming Window

The Hamming window is one of the most popular and most commonly used windows. Hamming window belongs to the family of raised cosine windows. The window is optimized to minimize the maximum (nearest) side lobe giving it a height of about one-fifth that of the Hann window, a raised cosine with simpler coefficients. A filter designed with the Hamming window has minimum stopband attenuation of 53dB. The transition region is somewhat wider than the stopband attenuation, which is considerably higher.

The Hamming window coefficients are expressed as:

$$W[n]=0.54-0.46\left(1-\cos\left(\frac{2\pi n}{N-1}\right)\right);0\le n\le N-1 \tag{33}$$

The magnitude response of the received signal after passing through the Hammimg window is shown in Fig. 22.

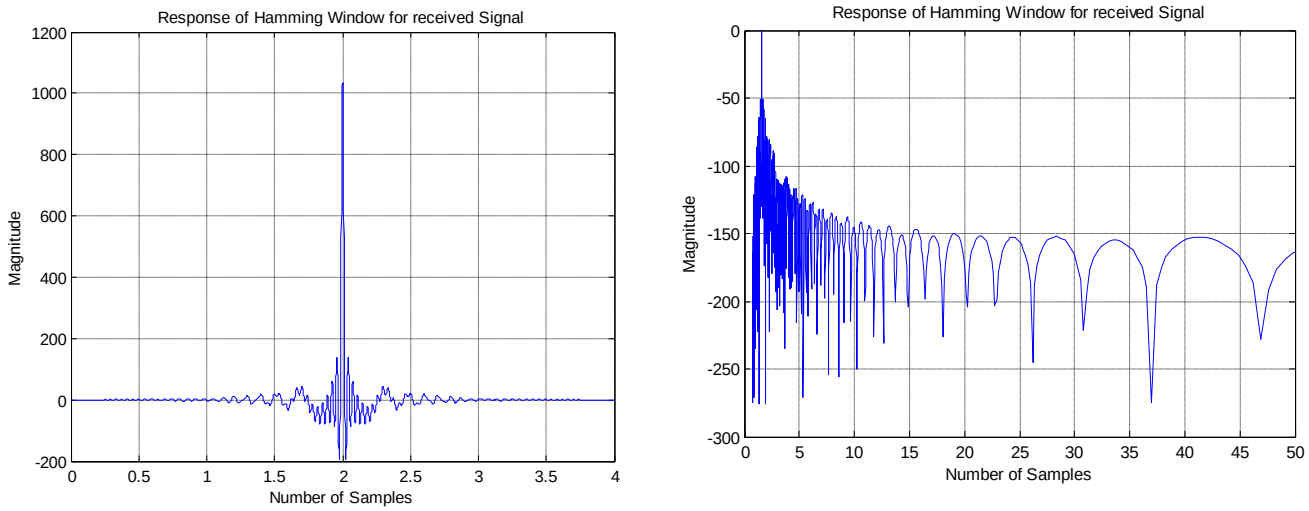

(a) Time domain (b) Frequency domain

Fig. 22 Magnitude response of received signal after hamming window

7.4 Kaiser Window

The windows described above are kind of a compromise between requirements for a narrow transition region (greater selectivity) and a higher stopband attenuation. All the windows described here are not optimal. An optimal window is a function that has maximum attenuation according to the given width of the main lobe. The optimal window is also known as Kaiser Window. Its coefficients are expressed as:

$$W[n] = \frac{I_0\left(\pi\alpha\left(\sqrt{1-\left(\frac{2n}{M}-1\right)^2}\right)\right)}{I_0(\pi\alpha)}, 0 \le n \le M$$

$$= 0 \qquad \text{otherwise} \qquad (34)$$

Where, I_0 is the zeroth order Modified Bessel function of the first kind and α is an arbitrary real number that determines the shape of the window. In the frequency domain, it determines the trade-off between main-lobe width and side lobe level, which is a central decision in the window design. M is an integer, and the length of the sequence is **N**=M+1.

The magnitude response of received signal after passing through the Kaiser window is shown in Fig. 23.

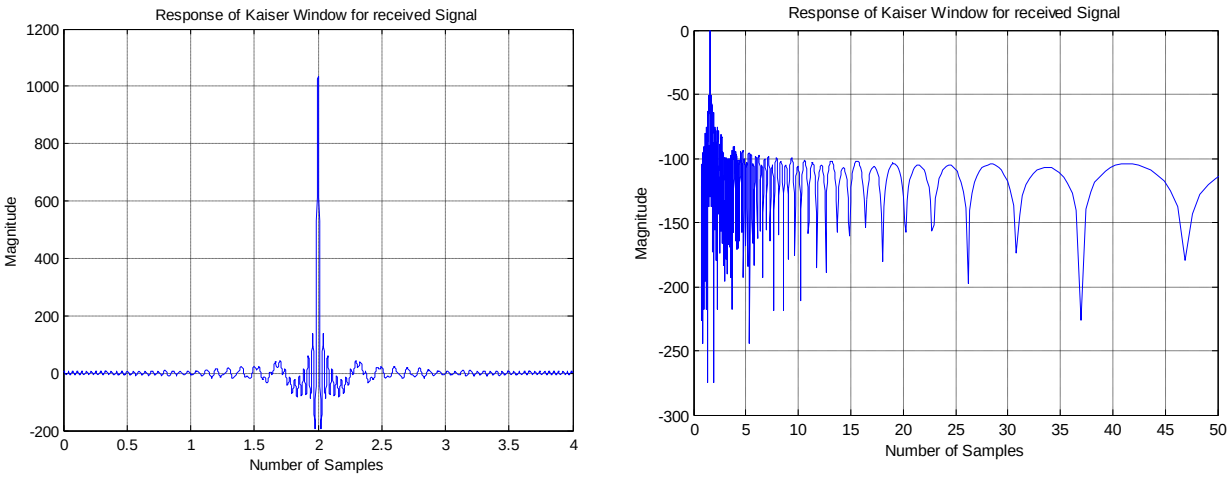

(a) Time domain (b) Frequency domain

Fig. 23 Magnitude response of received signal after Kaiser window

7.5 Blackman-Harris Window

The Blackman-Harris window is one of the most well-known and most commonly used windows. It is quite similar to Hann and Hamming window, but it has one additional cosine term to further reduce the ripple ratio. Blackman windows have slightly wider central lobes and less sideband leakage than the equivalent length of Hamming and Hann windows. It is characterized by high stop band attenuation and the widest transition region compared to all windows.

The Blackman-Harris window coefficients are expressed as:

$$W[n] = 0.35875 - 0.48829\cos\left(\frac{2\pi n}{N-1}\right) + 0.14128\cos\left(\frac{4\pi n}{N-1}\right) - 0.01168\cos\left(\frac{6\pi n}{N-1}\right); 0 \le n \le N-1 \quad (35)$$

The magnitude response of received signal after passing through the Blankman Harris window is shown in Fig. 24.

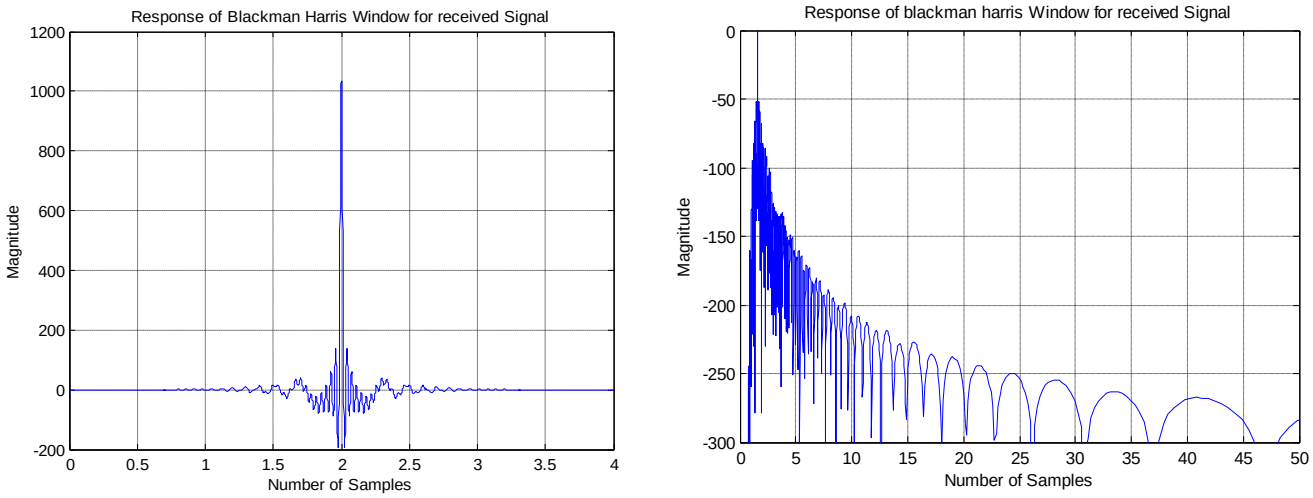

(a) Time domain (b) Frequency domain

Fig. 24 Magnitude response of received signal after Blackman Harris window

From above results it observed that by using Blackman Harris window, noise in the received signal of pulse compression sonar is reduced by a large value compared to all other window functions. In sonar applications, the Blackman-Harris window is the conventional choice. The Blackman-Harris window has good properties for low distortion and good sideband rejection.

Window technique	**Maximum side lobe level (dB)**	**Side lobe roll-off rate (dB/decade)**
Rectangular	13	20
Hann	31	40
Hamming	53	40
Kaiser	48	20
Blackman-Harris	71	60

Table 6 Comparison of windowing techniques for chirp sonar

From the Table 6, it is concluded that Blackman-Harris window performs better for chirp technology sonar with maximum side lobe level of 71dB and Side lobe Roll-off rate of 60 dB/decade.

8. Various Segmentation Methods

After the process of filtering, the next stage is segmentation where the objects are required to be identified. Image segmentation is generally an attempt to analyze or interpret an image.

Segmentation partitions an image into distinct regions those are meant to correlate strongly with objects or features of interest in the image. Segmentation can also be regarded as a process of grouping together pixels that have similar attributes (Xu, L., 2001, and Bell J.M., 2002). Segmentation is also responsible for bridging the gap between low level image processing and the high level image processing. The low level processing manipulates the pixel gray level to correct defects or enhance certain characteristics. The high level processing works with groups of pixels to represent particular features of interest. Some of the general image segmentation methods are: Clustering Methods, Histogram-Based Methods, Edge Detection Methods, Region Growing Methods, Level Set Methods, Graph Partitioning Methods, Watershed transformation, Model based Segmentation, Multi-scale Segmentation, Semi-automatic Segmentation, and Neural Networks Segmentation. For intensity images, there are four popular approaches which are threshold techniques, edge-based methods, region-based techniques, and connectivity-preserving relaxation methods. However, a single method may not be suitable for all applications (Fox W. L. J. et al, 2004; Reed et al, 2003). In this chapter, some of the segmentation methods are described in detail. These are applied to simulated sonar images and subsequently the results have also been tabulated. In the next section, the various segmentation methods will be described in detail.

8.1 Edge Detection

Edges are the clues towards the analysis and interpretation of image information. Sudden, sustained changes in image intensity are called edges. Edge detection is the process of determining which pixels are the edge pixels. The result is an edge map. Using this technique, one can extract the features of the objects either statically or dynamically. Edge detection of an image reduces significantly, the amount of data and filters out information that may be regarded as less relevant, preserving the important properties of an image. The edge detection methods can be grouped into two categories, search-based and zero-crossing based. The search-based methods detect edges by looking for maxima and minima in the first derivative of the image, usually local directional maxima of the gradient magnitude. The zero-crossing based methods search for zero crossings in the second derivative of the image. The various methods used in the edge detection can be classified as Gradient based Methods, Laplacian based methods or Diffusion based methods. The edge detection methods based on difference operation are also used in image processing. It could detect the variation of gray levels, but it is sensitive to noise. In order to improve the ability of noise rejection, a ratio of gray levels between two successive image points is used to denote the variation of gray levels. The

advantage of this detection method is that the sensitivity of edge detection can be adjusted easily. The results have shown that the effectiveness of edge detection and the ability of noise rejection of this method are better than that of the traditional methods based on the difference operation.

Analysis:

i) The method is based on the difference operation between adjacent pixels

ii) It works better than conventional difference based edge detectors

iii) It can accurately detect edges even in the presence of strong noise

iv) Computational time is greater than that of other edge detection methods

8.2 Canny's Edge Detection

The Canny Edge Detection Algorithm follows the steps given below

i) Smooth the image with a Gaussian filter,

ii) Compute the gradient magnitude and orientation using finite difference approximations for the partial derivatives,

iii) Apply non-maxima suppression to the gradient magnitude,

iv) Use the double thresholding algorithm to detect and link edges.

v) Canny edge detector approximates the operator that optimizes the product of signal-to-noise ratio and localization. It is generally the first derivative of a Gaussian. The first step in the algorithm is the smoothing of the image with a Gaussian filter. Let I[i, j] denote the image, G[i, j; σ] be a Gaussian smoothing filter where σ is the spread of the Gaussian and controls the degree of smoothing. The result of convolution of I[i,j] with G[i, j; σ] gives an array of smoothed data as

$$S[i,j] = G[i,j,\sigma] * I[i,j] \tag{36}$$

The second step is the calculation of the gradient magnitude and direction. Firstly, the gradient of the smoothed array S[i ,j] is used to produce the x and y partial derivatives P[i ,j] and Q[i, j] respectively as

$$P[i,j] \approx \{S[i,j+1] - S[i,j] + S[i+1,j+1] - S[i+1,j]\}/2 \tag{37}$$

$$Q[i,j] \approx \{S[i,j] - S[i+1,j] + S[i,j+1] - S[i+1,j+1]\}/2 \tag{38}$$

The x and y partial derivatives are computed by taking the average of the finite differences over the 2x2 square. From the standard formulas for rectangular-to-polar conversion, the magnitude and orientation of the gradient can be computed as

$$M[i,j] = \sqrt{P[i,j]^2 + Q[i,j]^2} \quad (39)$$

$$\theta[i,j] = \arctan(Q[i,j], P[i,j]) \quad (40)$$

Here the arctan(x,y) function takes two arguments and generates an angle.

The third step is the application of non-maxima suppression to the gradient magnitude. Given the magnitude of image array, one can apply the thresholding operation in the gradient-based method and end up with ridges of edge pixel. But C anny has a more sophisticated approach to the problem. In this approach an edge point is defined to be a point whose strength is locally maximum in the direction of the gradient. This is a stronger constraint to satisfy and is used to thin the ridges found by thresholding. This process, which results in one pixel wide ridges, is called "Non-maxima Suppression". After non-maxima suppression one ends up with an image $N[i,j] = nms(M[i,j], \zeta[i,j])$ which is zero everywhere except at the local maxima points. At the local maxima points the value of pixels is preserved.

Analysis:

The Canny operator looks to satisfy three criteria:

i) Good detection: low probability of missing real edges, and low probability of detecting non-existent edges

ii) Good localization: points determined to be edge points are close to the true edge points

iii) Only one response: detecting each edge only once

iv) It has high PSNR value

8.3 Adaptive Thresholding

Thresholding is the process of selecting a gray level, which will serve as a threshold to distinguish the two classes in the image i.e., objects and their background. The thresholded product is achieved by scanning the original image, pixel by pixel, and testing each pixel against the selected threshold i.e, if f(x, y)>Th, then the pixel is classified as a background pixel, otherwise the pixel is classified as an object pixel (Satya Swaroop Pradhan et al, 2008). This can be summarized in the following definition, where b(x, y) denotes the thresholded binary image:

$$b(x,y) = \begin{cases} 255, if\ f(x,y) \geq Th \\ 0, if\ f(x,y) \leq Th \end{cases} \quad (41)$$

where,

f(x , y) is the pixel intensity at a point (x, y) in the original image.

To understand the idea of adaptive thresholding, consider the case when the illumination is non uniform i.e, some part of the image is extremely bright and the other part is affected by noise and shading. Then applying a single threshold to the entire image may result in loss of detecting certain objects . So, there is a need to apply a threshold value which varies adaptively taking into consideration the effects of illumination and noise. This method is known as adaptive thresholding. The general definition of a threshold can be written in the following manner

$$Th = Th\,[x, y, p(x, y), f(x, y)] \quad (42)$$

where,

f(x, y) = gray level of point (x, y) in the original image,

p(x, y) = some local property of this point.

When Th depends only on the gray-level at that point, then it degenerates into a simple global threshold. The factor, p(x, y) is an important component in the calculation of the threshold for a certain point (Martinez G., 2005; Kumar M N V S S).

The algorithm of Adaptive Thresholding method is summarized in the following steps

i) Smooth the image by average filtering

ii) Derive the gray level gradient magnitude

iii) Apply thresholding and a thinning algorithm to the gradient magnitude to find the object boundary points

iv) Sample the smoothed image at the boundary points as local thresholds

v) Interpolate the threshold surface by sampled local thresholds

vi) Segment the image by the threshold surface.

Analysis:

i) In this method, first the image was divided into a regular grid of non overlapping sub regions and a threshold is assigned to the centre of each sub region.

ii) Then the threshold surface is interpolated from these local threshold values.

iii) Adaptive thresholding enables the neighbourhood compactness technique to pick up straight edges that are of 1 pixel width without incurring significant noise.

iv) Computation time is less compared to other conventional methods.

v) It is not suitable when noise is too high. Its peak SNR value is also very low.

8.4 Fuzzy C Means Thresholding

Fuzzy clustering is the oldest fuzzy approach to image segmentation. Algorithms such as Fuzzy C-means (FCM) and Possibilistic C-means can be used to build clusters (segments). The class membership of pixels can be interpreted as similarity or compatibility with an ideal object or a certain property. Fuzzy C-means Clustering (FCM), also known as Fuzzy ISODATA, is also clustering technique. The FCM employs fuzzy partitioning such that a data point can belong to all groups with different membership grades between 0 and 1. FCM is an iterative algorithm. The aim of FCM is to find cluster centres (centroids) that minimize a dissimilarity function. To accommodate the introduction of fuzzy partitioning, the membership matrix (U) is randomly initialized according to

$$\sum_{i=1}^{c} u_{i,j} = 1, \forall j = 1, \ldots\ldots, n \tag{43}$$

The dissimilarity function which is used in FCM is given by

$$J(U, c_1, c_2, \ldots\ldots, c_c) = \sum_{i=1}^{c} J_i = \sum_{i=1}^{c} \sum_{j=1}^{n} u_{ij}^{m} d_{ij}^{2} \tag{44}$$

where,

u_{ij} is between 0 and 1

c_i = centroid of cluster i

d_{ij} = Euclidian distance between i_{th} centroid(c_i) and j_{th} data point

m ϵ [1,∞] is a weighting exponent.

To reach a minimum of dissimilarity function, there are two conditions. These are given in (4.27) and (4.28).

$$c_i = \frac{\sum_{j=1}^{n} u_{ij}^{m} x_j}{\sum_{j=1}^{n} u_{ij}^{m}} \tag{45}$$

$$u_{ij} = \frac{1}{\sum_{k=1}^{c} \left(\frac{d_{ij}}{d_{kj}} \right)^{\frac{2}{(n-1)}}} \tag{46}$$

The Fuzzy C-means algorithm is as follows

i) Randomly initialize the membership matrix (U) that has constraints in Eq. (43).

ii) Calculate centroids (c_i) by using Eq. (45).

iii) Compute dissimilarity between centroids and data points using Eq. (44).And stop if its improvement over previous iteration is below a threshold.

iv) Compute a new membership matrix (U) using Eq. (46). Go to Step 2.

By iteratively updating the cluster centres and the membership grades for each data point, FCM iteratively moves the cluster centres to the "right" location within a data set. FCM does not ensure that it converges to an optimal solution.

Performance of depends on the initial centroids. For a robust approach there are two ways which are described below.

i) Using an algorithm to determine all of the centroids. (for example: arithmetic means of all data points)

ii) Run FCM several times each starting with different initial centroids.

Analysis:

i) It is an unsupervised form of cluster analysis.

ii) It is a generalization of classical K means or Hard C- Means algorithm and works better than K means.

iii) The FCM thresholding method is capable of segmenting an image in the presence of reverberation noise.

iv) The FCM algorithm is robust and it is sensitive to slightest changes in the image.

v) One of the main drawbacks of FCM thresholding is the computation time.

8.5 Adaptive histogram equalization

In image processing, the histogram of an image normally refers to a histogram of the pixel intensity values. This histogram is a graph showing the number of pixels in an image at each different intensity value found in that image. Histograms have many uses. One of the more common ones is to decide what value of threshold to use when converting a grayscale image to a binary image by thresholding. If the image is suitable for thresholding, then the histogram will be bi-modal i.e, the pixel intensities will be clustered around two well-separated values. A suitable threshold for separating these two groups will be found somewhere in between the two peaks in the histogram (Fig. 25).

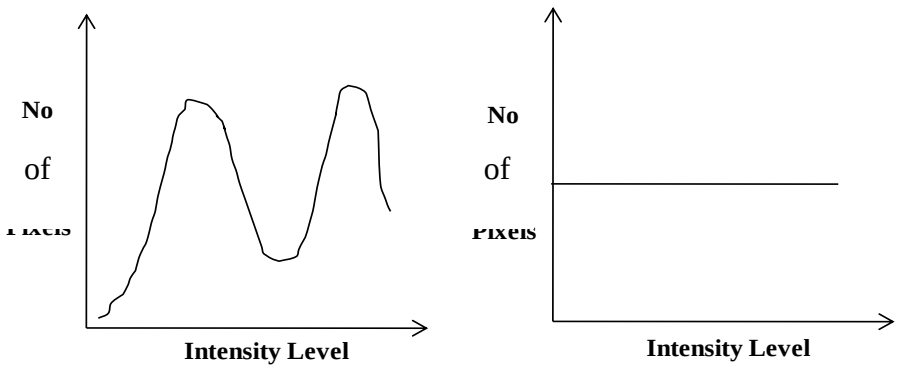

Typical Histogram **Ideal Histogram**

Fig. 25 Depiction of typical and ideal histograms

Traditionally, histogram equalization is also a global technique in the sense that the enhancement is based on the equalization of the histogram of the entire image (Fig. 26). However, it is well recognized that using only global information is often not enough to achieve good contrast enhancement.

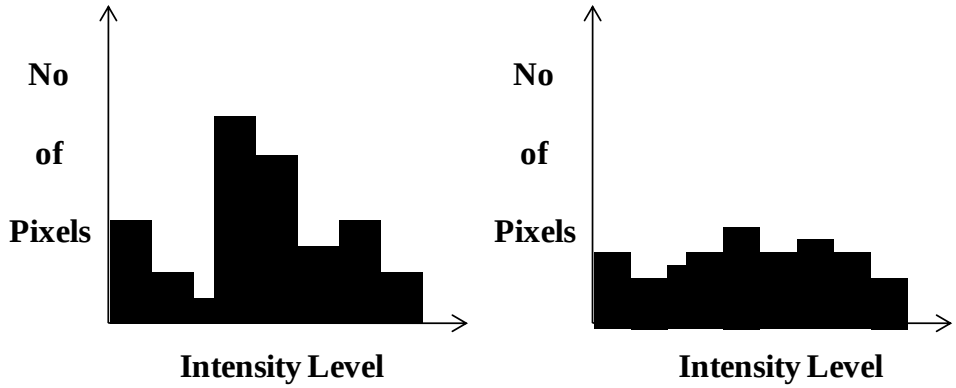

Fig. 26 Depiction of histograms before and after equalization

Adaptive histogram equalization differs from ordinary equalization in that the adaptive method computes several histograms, each corresponding to a distinct section of the image, and uses them to redistribute the lightness values of the image. Ordinary histogram equalization simply uses a single histogram for an entire image. To correct this problem, adaptive histogram equalization is used, which considers a local window for each individual pixel and computes the new intensity value based on the local histogram defined in the local window. The algorithm of Adaptive Histogram equalization is given below.

i) Obtain all the inputs:

a. image

b. number of regions in row and column directions

c. number of bins for the histograms used in building image transform function

d. clip limit for contrast limiting (normalized from 0 to 1)

ii) Pre-process the inputs:

a. determine real clip limit from the normalized value

b. if necessary, pad the image before splitting it into regions

iii) Process each contextual region (tile) thus producing gray level mappings

a. extract a single image region

b. make a histogram for this region using the specified number of bins

c. clip the histogram using clip limit

d. create a mapping (transformation function) for this region

iv) Interpolate gray level mappings in order to assemble final CLAHE image

a. extract cluster of four neighbouring mapping functions

b. process image region partly overlapping each of the mapping tiles

c. extract a single pixel, apply four mappings to that pixel, and

d. interpolate between the results to obtain the output pixel;

e. repeat over the entire image

Analysis:

i) The adaptive histogram equalization method computes several histograms, each corresponding to a distinct section of the image.

ii) It is capable of improving an image's local contrast, bringing out more detail in the image.

iii) Each region's histogram is enhanced so that the histogram of a specific region matches that of the original one.

iv) For the simulated image, the above method yields high PSNR value and low computation time.

When all the above mentioned methods were subjected to real sonar images, it was observed that none of the method is able to segment the images as per the required standard. Many false alarms were being detected in the images. Subsequently a new algorithm was proposed which was best suited to the underwater images.

9. Results of Image Segmentation

The results of segmentation using the various existing methods and the proposed design method are shown below.

9.1 Basic Edge Detection

This method is based on the difference operation between adjacent pixels. This method can accurately detect edges even in the presence of strong noise. In this method the computational time is greater than that of other edge detection methods (Fig. 27)

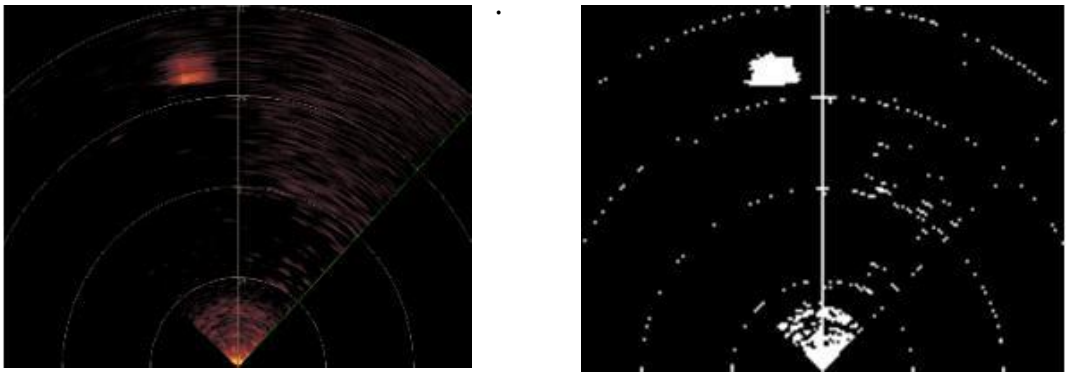

(a) Input Image (b) Output Image

Fig. 27 Results of the Edge detection method

9.2 Canny Edge Detection

This method has low probability of missing the real edges and detecting non-existent edges. This method has two major advantages ,one is that it detects each edge only once and the other one is having high PSNR value (Fig. 28).

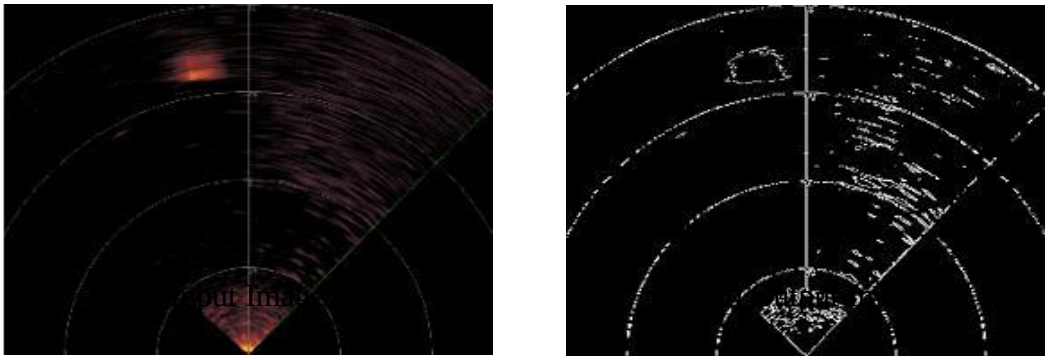

Fig. 28 Results of the Canny Edge detection method

9.3 Adaptive Thresholding

In this method, first the image was divided into a regular grid of non overlapping sub regions and a threshold is assigned to the center of each sub region followed by interpolation of threshold surface from these local threshold values.

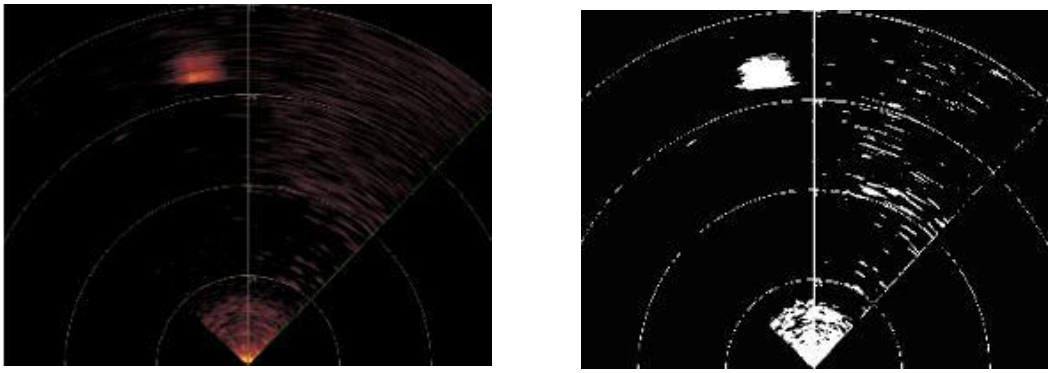

(a) Input Image (b) Output Image

Fig. 29 Results of the adaptive thresholding method

This method enables the neighbourhood compactness technique to pick up straight edges that are of 1 pixel width, without incurring significant noise. Here computation time is less compared to other conventional methods. This method is not suitable when noise is too high and its PSNR value is also very low (Fig. 29).

9.4 Fuzzy C Means thresholding

It is an unsupervised form of cluster analysis, which is a generalization of classical K means or Hard C- Means algorithm. This method is capable of segmenting an image in the presence of reverberation noise. The FCM algorithm is robust. However, it is sensitive to slightest changes in the image. The main drawback of this method is the large computation time (Fig. 30).

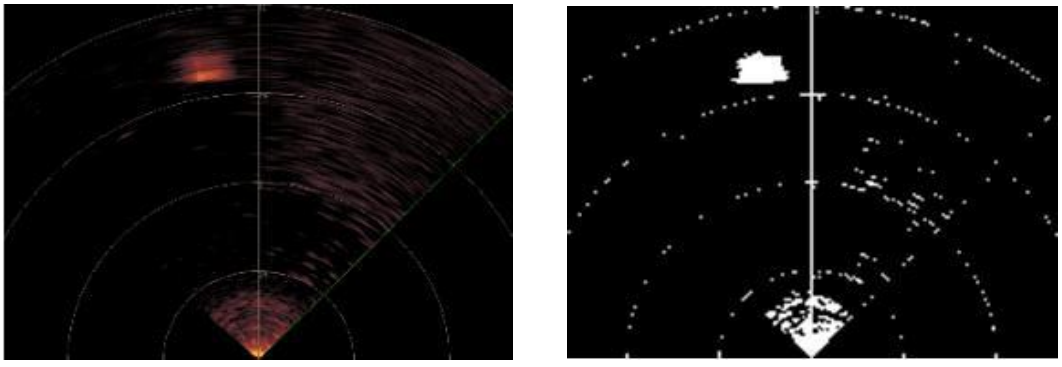

(a) Input Image (b) Output Image

Fig. 30 Results of the Fuzzy – C means thresholding method

9.5 Adaptive Histogram Equalization

This method computes several histograms, each corresponding to a distinct section of the image. This method improves the image's local contrast thereby bringing out more detail in the image.

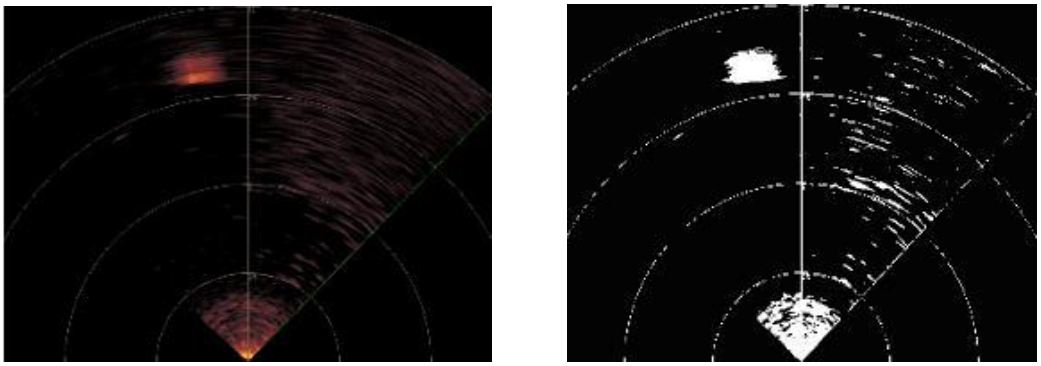

(a) Input Image (b) Output Image

Fig. 31 Results of the adaptive histogram equalization method

Each region's histogram is enhanced so that the histogram of a specific region matches that of the original one (Fig. 31). The Execution time and the Peak SNR (PSNR) that have been achieved in respect of the existing methods have been depicted in Table 7.

S. No.	Method	Execution time (sec)	PSNR (dB)
1	Adaptive thresholding	0.720207	0.3037
2	Edge detection based on difference technique	4.242526	13.4538
3	Canny edge detection	1.109931	12.6053
4	FCM thresholding	212.157879	9.6658
5	Adaptivehistogram equalization	2.1358	15.0972

Table 7 Execution time and PSNR in respect of the existing methods

10. Principal Components Analysis (PCA)

Principal Components Analysis (PCA) is a way of identifying patterns in data, and expressing the data in such a way to highlight their similarities and differences. Since patterns recognition in high dimensional data is very difficult, where the luxury of graphical representation is not available, PCA is a powerful tool for data analysis and pattern recognition which is often used in signal and image processing as a technique for data

compression, data dimension reduction, (i.e. by reducing the number of dimensions, without much loss of information) or their decorrelation as well. In this section, the steps needed to perform a Principal Components Analysis on a set of data are discussed. It covers standard deviation, covariance, eigen vectors and eigen values. This background knowledge is meant to make the PCA section very straightforward.

10.1 Covariance

Covariance is a measure of how much two random variables change together, which is always measured between 2 dimensions. If the covariance is measured between one dimension, i.e., with itself, then it is known as variance. Therefore, if a 3-dimensional data set (x, y, z), is considered then it could measure the covariance between the x and y dimensions, the x and z dimensions, and the y and z dimensions. Measuring the covariance between x and x or y and y or z and z would give the variance of the x, y and z dimensions respectively. The formula for covariance is similar to the formula for variance. The formula for covariance between 2-dimensional data set of length, *n* can be written as:

$$\operatorname{cov}(X,Y) = \frac{\sum_{i=1}^{n} (X_i - \bar{X})(Y_i - \bar{Y})}{n-1} \tag{47}$$

If the covariance value is positive, then it indicates that both dimensions increase together. If the value is negative, then as one dimension increases, the other decreases. In the last case, if the covariance is zero, it indicates that the two dimensions are independent of each other. This technique is often used to find relationships between dimensions in high-dimensional data sets where visualization is difficult (Lindsay I Smith., 2002; Yi Zhou., 2010).

10.2 The Covariance Matrix

If a data set with more than 2 dimensions is considered, there is more than one covariance measurement that can be calculated. For example, from a 3 dimensional data set (dimensions x, y, z) it could calculate *cov*(x, y), *cov*(x,z) and *cov*(y,z). In fact, for a n-dimensional data set, it calculates $\frac{n!}{(n-2)!2}$ different covariance values (Jun Zhang, 1997).

A useful way to get all the possible covariance values between all the different dimensions is to calculate them all and put them in a matrix. So, the definition for the covariance matrix for a set of data with n-dimensions is:

$$C^{n\times n} = (c_{i,j}, c_{i,j} = \text{cov}(Dim_i, Dim_j)) \tag{48}$$

Where, $C^{n\times n}$ is a matrix with n rows and n columns and each entry in the matrix is the result of calculating the covariance between two separate dimensions.

10.3 Eigen vectors

Let A be a $n\times n$ matrix. The eigen values of A are defined as the roots of:

$$\text{Determinant}(A - \lambda I) = |A - \lambda I| = 0 \tag{49}$$

where, is the $n\times n$ identity matrix. This equation is called the characteristic equation (or characteristic polynomial) and has n roots.

Let λ be an eigen value of A. Then there exists a vector x such that:

$$Ax = \lambda x \tag{50}$$

The vector x is called an eigenvector of A associated with the eigen value, λ. There is no unique solution for x in the above equation. It is a direction vector only and can be scaled to any magnitude. To find a numerical solution for x it is necessary to set one of its elements to an arbitrary value, say 1, which gives a set of simultaneous equations to solve for the other elements. If there is no solution, the process should be repeated with another element (Howard Anton, 2006). Ordinarily the final values are normalized so that x has length 1 that is $x.x^T = 1$

Consider a 3×3 matrix A with eigenvectors x_1, x_2, x_3 and eigen values $\lambda_1, \lambda_2, \lambda_3$ so then

$$Ax_1 = \lambda x_1, \qquad Ax_2 = \lambda x_2, \qquad Ax_3 = \lambda x_3 \tag{51}$$

Putting the eigenvectors as the columns of a matrix gives:

$$A\begin{bmatrix} x_1 & x_2 & x_3 \end{bmatrix} = \begin{bmatrix} x_1 & x_2 & x_3 \end{bmatrix}\begin{bmatrix} \lambda_1 & 0 & 0 \\ 0 & \lambda_2 & 0 \\ 0 & 0 & \lambda_3 \end{bmatrix} \tag{52}$$

let

$$\Phi = \begin{bmatrix} x_1 & x_2 & x_3 \end{bmatrix} \qquad \Lambda = \begin{bmatrix} \lambda_1 & 0 & 0 \\ 0 & \lambda_2 & 0 \\ 0 & 0 & \lambda_3 \end{bmatrix} \tag{53}$$

From Eqs. (52) and (53), the matrix equation can be written as

$$A\Phi = \Phi\Lambda \tag{54}$$

Then normalizing the eigenvectors to unit magnitude, as they are orthogonal, so:

$$\Phi\Phi^T = \Phi^T\Phi = 1 \tag{55}$$

which means that

$$\Phi^T A\Phi = \Lambda$$

and

$$\Phi^T \Lambda\Phi = A \tag{56}$$

11. PCA fusion

Image fusion is 'the combination of two or more different images to form a fused image by using a fusion algorithm'. In this, an algorithm is designed in which the pixels are extracted from the stacked images. Principal component analysis is carried out on these pixels which aim at reducing a large set of variables to a small set that still containing most of the information that was available in the large set. The technique of principal component analysis enables us to create and use a reduced set of variables, which are called principal factors. A reduced set is much easier to analyze and interpret.

11.1 Steps to carry out PCA on sonar images

Extract relevant information in an image (Principal Components) and encode that information in a suitable data structure.

Step 1: Get data sets from different images

Step 2: Normalize/adjust the data (subtract the mean). For PCA to work properly, subtract the mean from each of the data dimensions. The mean subtracted is the average across each dimension.

Step 3: Calculate the covariance matrix

Step 4: Calculate the eigen vectors and eigen values of the covariance matrix. There can be many eigen vectors for a covariance matrix but very few of them are the principle ones. Although each eigen vector can be used for finding different amount of variations among the image, only principal eigen vectors are considered because these can account for substantial variations among a bunch of images which shows the most significant relationship between the data dimensions. By this process of taking the eigen vectors of the covariance matrix, the lines that characterize the data can be extracted.

Step 5: Choosing components and forming a feature vector

In general, once eigen vectors are found from the covariance matrix, the next step is to order them by eigen value, highest to lowest. This gives the components in their order of significance and to ignore the components of lesser significance because of which some information can be lost if the eigen values are small, don't lose much information. After leaving out some components, the final data set will have fewer dimensions than the original. To be precise, consider original data having *n* dimensions and then get *n* eigen vectors and eigen values for given data, and then choose only the first *p* eigenvectors. Now the final data set has only *p* dimensions. So forming a matrix with these eigenvectors in the columns and the matrix is called *feature vector*.

$$\text{Feature vector} = (\text{eig}_1\ \text{eig}_2\ \text{eig}_3\ \ldots\ldots \text{eig}_n) \quad (57)$$

Step 6: Deriving the new data set

The final data is obtained simply by taking the transpose of the feature vector and multiply it on the left of the original data set, transposed.

$$\text{Final data} = \text{Row feature vector} \times \text{Row data adjust} \quad (58)$$

where ,Row feature vector is the matrix with the eigen vectors in the columns *transposed* so that the eigen vectors are now in rows, with the most significant eigen vector at the top, and the Row data adjust is the mean-adjusted data *transposed*, i.e. the data items are in each column, with each row holding a separate dimension.

12. New Image Synthesis Algorithm for Under Water Object Identification

This algorithm mainly involves two steps (i) Quality assessment of spatial domain and (ii) Sonar image synthesis using quality assessment

(i) Quality assessment of Spatial Domain

Quality assessment of images has been successfully employed in the authentication area, such as iris and fingerprint verification, which is used to evaluate the quality of the captured images. Fingerprint quality is usually defined as a measure of the clarity of the ridge and valley structures. In the multi-focus image fusion, it is the first step to investigate whether the region of the image has clarity or not, so the quality assessment is incorporated into multi-focus image synthesis algorithm. Generally, the quality assessment can be classified into two ways, namely the frequency domain assessment and the spatial domain assessment. The latter one is incorporated into this algorithm (Kumar M N V S S, et al.,2012).

In order to assess the image quality in a local region, a given image is partitioned into a lattice of blocks of size $b \times b$. For each block, B let $g_s=(g_s^x, g_s^y)$ denote the gradient of the

gray level intensity at site $s \in B$. The covariance matrix, J of the gradient vectors for all b^2 sites in this B block is given by

$$J=\frac{1}{b^2}\sum_{s\in B} g_s^T g_s = \begin{bmatrix} j_{11} & j_{12} \\ j_{21} & j_{22} \end{bmatrix} \quad (59)$$

The above symmetric matrix is positive semi definite with Eigen values

$$\lambda_1=\frac{1}{2}\left(trace(J)+\sqrt{trace(J)-4\det(J)}\right)$$
$$\lambda_2=\frac{1}{2}\left(trace(J)-\sqrt{trace(J)-4\det(J)}\right) \quad (60)$$

Where, trace (J) $=j_{11}+j_{22}$, det (J)$= j_{11}j_{22}-j^2_{12}$ and $\lambda_1 \geq \lambda_2$.

The quality assessment is defined as

$$\lambda = \lambda_1 - \lambda_2 \quad (61)$$

This measure reflects the clarity of the local region. The clearer the local region is, the bigger the measure will be (Wang. et al., 2004).

(ii) Sonar Image Synthesis using quality assessment

The block diagram for sonar image synthesis is shown in Fig. 32. The algorithm for the sonar image synthesis using quality assessment is as follows:

The images obtained by different segmentation methods of a sonar image are fused into a single image having all objects in focus without producing details that are non-existent in the given images. The algorithm consists of the following steps:

- Let I^1, I^2...I^5 be the noisy images of an object obtained by various segmentation methods applied to a sonar image *S*. Let I^i be of size $N \times N$ where $i = 1, 2, \ldots 5$.
- The images I^i for $i=1,2,..,5$ are divided into non-overlapping rectangular blocks (or regions) with size of $m \times n$. The j^{th} image blocks of I^i are referred by I^i_j.
- Quality assessment value (λ) of I^i_j is calculated and the results of I^i_j are denoted by λ^i_j.

In order to determine the sharper image block, the quality assessment value of image blocks from *5* noisy images are sorted in descending order and the same ordering is associated with image blocks. The block with the maximum quality assessment is kept in the fused image. The fusion mechanism is represented as follows:

If λ^i_j is the quality assessment value of block I^i_j, the ordering of assessment values is given by

$$\lambda_{(1)} > \lambda_{(2)} > \ldots\ldots > \lambda_{(5)}$$

and this implies the same ordering to the corresponding blocks

$$I_{(1)} > I_{(2)} > \ldots > I_{(5)}$$

where the subscripts are the ranks of the image blocks. Since the block with the largest quality assessment value is in the fused image, it will correspond to rank 1 of the ordered blocks, i.e. $Fused\ Block = I_{(1)}$

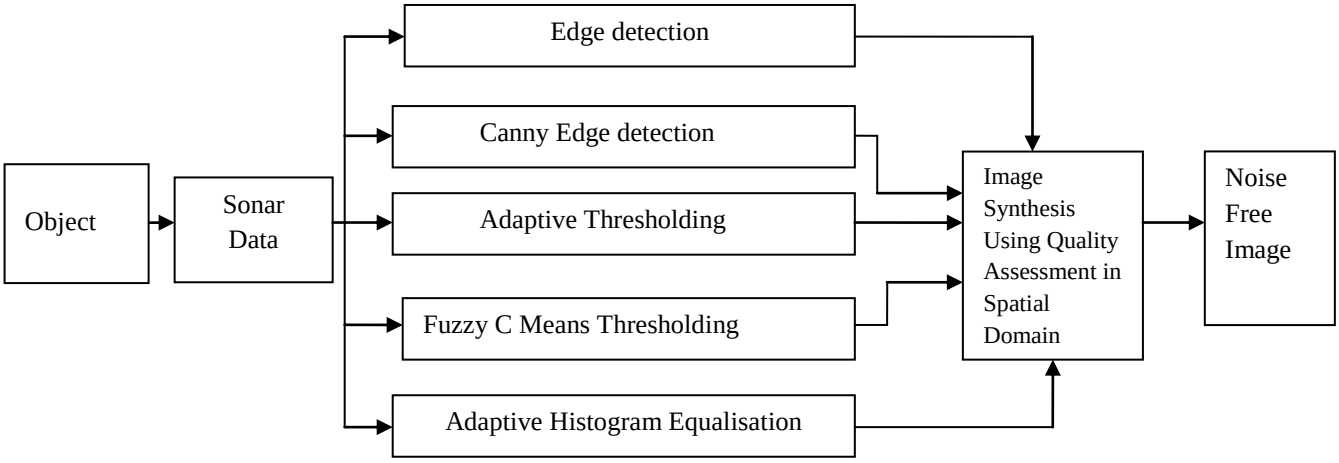

Fig. 32 Block diagram of sonar image synthesis

Fig. 32 shows the fusion of five noisy images obtained by various segmentation methods i.e., Edge detection, Canny Edge detection, Thresholding, Fuzzy C Means Thresholding and Adaptive Histogram Equalization into a single image retaining the important features of each image (Kumar M N V S S, et al.,2012).

13. Image Quality measures

There are two main methodologies those are used to estimate the quality of images. They are subjective evaluation and objective evaluation.

(i) Subjective evaluation

As the final users of most images are humans, the most reliable and commonly used assessment of image quality, is therefore subjective rating by observers. So as to obtain reliable quality rating, subjective viewing tests have been carried on post processed images. The rating for given image has been marked as excellent, good, average, bad etc. The result of given rating depends on the following factors.

a) The experience and motivation of the subject.

b) The range of the picture used,

c) The conditions under which the pictures are viewed (ambient illumination, contrast ratio, viewing distance)

(ii) Objective quality measures

The simplest and most commonly used objective measures are Mean Square Error (MSE) and the Peak Signal to Noise Ratio (PSNR). The mathematical formulae for the two are

$$MSE = \frac{1}{MN}\sum_{y=1}^{M}\sum_{x=1}^{N}[I(x,y) - I^{1}(x,y)]^{2} \quad (62)$$

$$PSNR = 20\times \log_{10}(255 / \text{sqrt}(MSE)) \quad (63)$$

Where I(x,y) is the original image, I'(x,y) is the approximated version and M,N are the dimensions of the images. These measures give simple mathematical deviation between original image and reconstructed image. They operate solely on pixel by pixel basis. Image with lower MSE and a high PSNR, signifies that the image is a relatively better one. The obvious drawback of MSE is its inability to reflect Human Visual System (HVS) [13]. Due to its shortcoming, many researchers have been searching better Image Quality Assessment (IQA) algorithms. During the past years, researchers have proposed several full reference Image Quality Assessment (IQA) algorithms which aim to reflect the perception of human eyes. One of them is Structural Similarity Index Measure (SSIM).

14. Results and Discussion

The input and segmented images of various methods mentioned are shown in Fig. 33. The experimental setup for collecting the data is shown in Fig. 33.

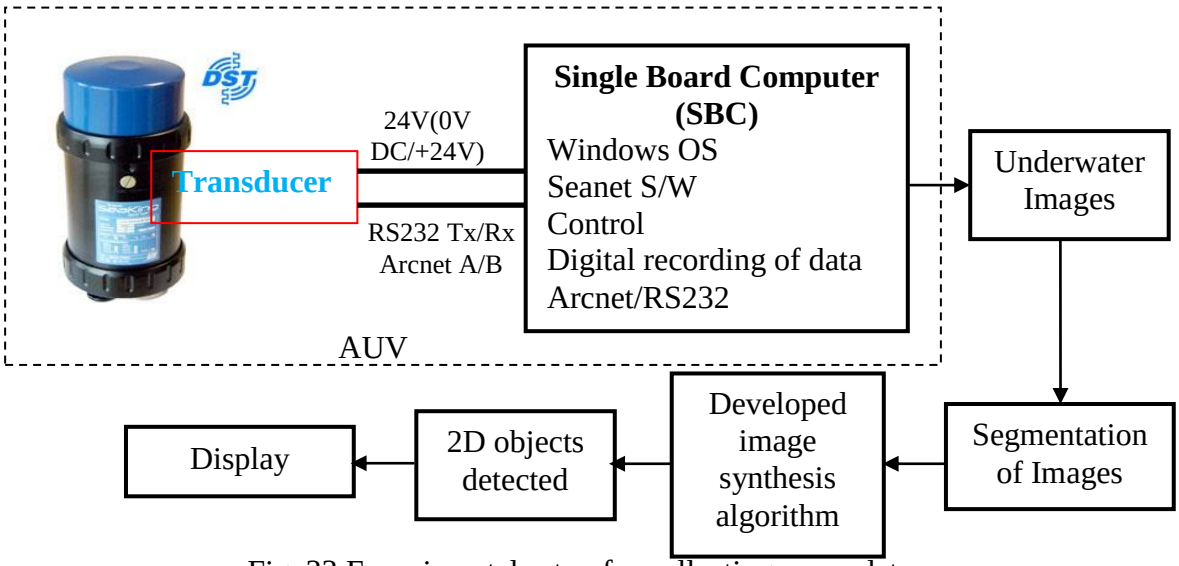

Fig. 33 Experimental setup for collecting sonar data

The sonar images obtained at various locations are considered for implementing the existing methods, Edge detection, Canny Edge detection, Adaptive Thresholding, Fuzzy – C means

thresholding, Adaptive Histogram Equalization and the proposed PCA and image synthesis algorithm. The segmented images for the existing methods are shown in Fig. 34. Fig. 34 (a) represents real time sonar image, Fig. 34 (b) represents Edge detection output, Fig. 34 (c) represents Canny Edge detection output, Fig. 34 (d) represents Adaptive Thresholding output, Fig. 34 (e) represents Fuzzy – C means thresholding output, and the Fig. 34 (f) represents Adaptive Histogram Equalization output.

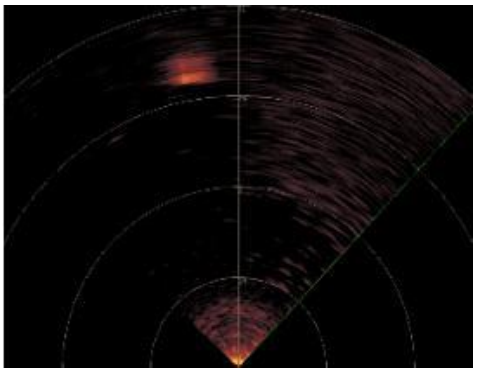

Fig. 34 (a) Real time sonar image

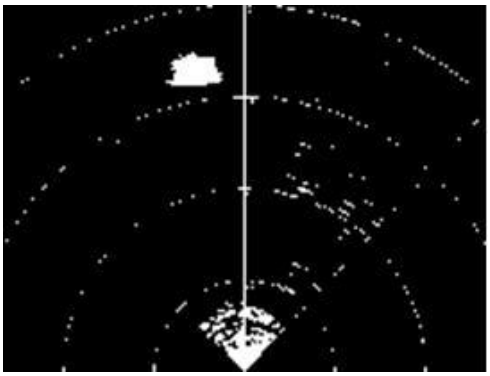

Fig. 34 (b) Results of the Edge detection method

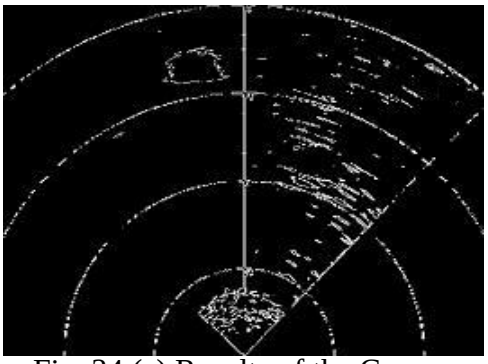

Fig. 34 (c) Results of the Canny Edge detection method

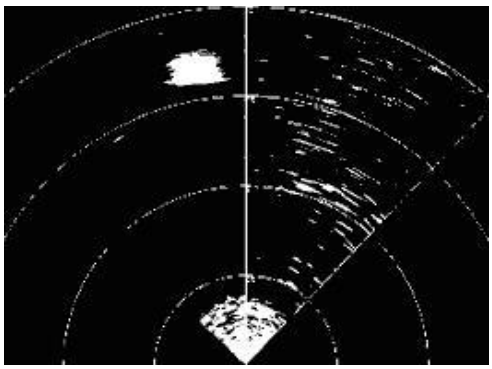

Fig. 34 (d) Results of the adaptive thresholding method

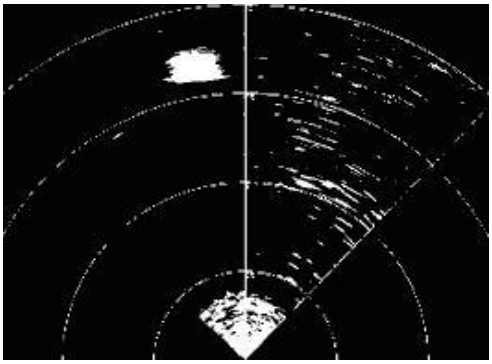

Fig. 34 (e) Results of Fuzzy – C means thresholding method

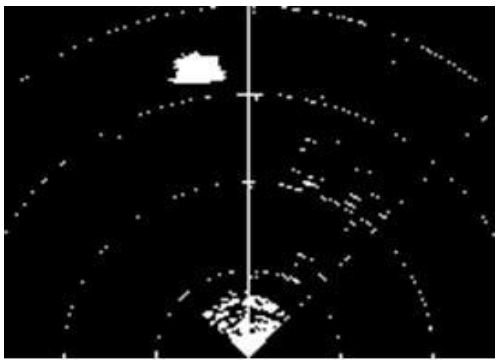

Fig. 34 (f) Results of adaptive histogram equalization method

It can be seen that the results shown above contain noise along with object information. Even after applying various segmentation techniques and image processing techniques the object is not detected clearly. Lot of noise is still present along with the object of interest. So in order to remove the noise, the results of all segmentation methods implemented are combined into single image so as to sustain the features of individual segmented image. This is done by using Principal Component Analysis method. In this method, the image being two dimensional, first the mean of each dimension is subtracted from the dimensions of the image. This makes zero mean of data set. Now the covariance is calculated for this data set. Subsequently, eigen vectors and eigen values are calculated for the covariance matrix. After finding the eigen vectors they are ordered based on the eigen values. This process is performed for all segmented images. After this, the data set having higher Eigen values are chosen and the same are multiplied with their corresponding data set. This provides the new data set, which is formed from all segmented images. The image formed by this data set is shown in Fig. 35. From this figure it is observed that the noise is further reduced. However it can also be observed that even after applying various segmentation methods and PCA the image still contains noise. In order to remove the noise completely, a new image synthesis algorithm has therefore been developed. In this algorithm, all segmented images are combined into single image by retaining all the features of image processing methods previously implemented. The goal of image synthesis algorithm is to create new images that are more suitable for the purpose of human visual perception, object detection and target recognition. The use of multiple images has led to improved recognition rate in applications such as automatic target recognition. In this process the segmented images are synthesized for identifying the image clearly and the result has been shown in Fig. 36. The existing segmentation methods, PCA and the developed algorithm are compared in terms of PSNR and the results are given in Table 8. It is observed that the proposed algorithm has better PSNR of 38.006dB.

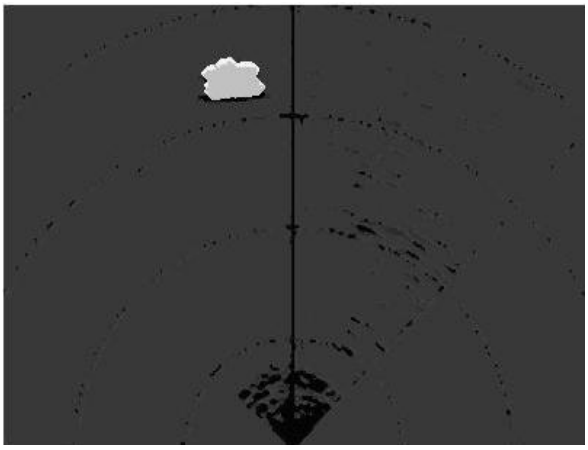

Fig. 35 Results of the principle component analysis method

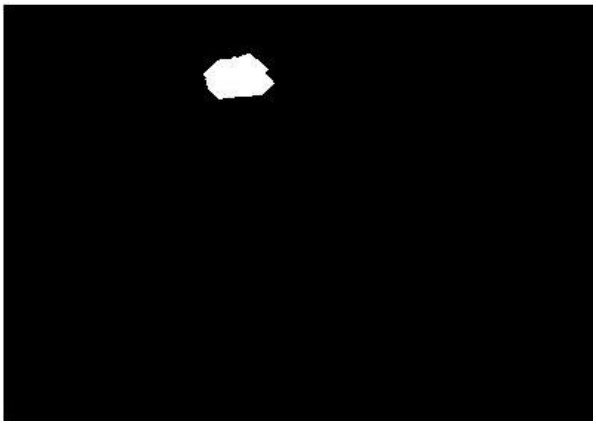

Fig. 36 Results of image synthesis method

Table 8 Comparison of various existing segmentation methods and developed algorithm

S. No.	Method	Execution time (sec)	PSNR (dB)
1	Adaptive thresholding	0.720207	0.3037
2	Edge detection based on difference technique	4.242526	13.4538
3	Canny edge detection	1.109931	12.6053
4	FCM thresholding	212.157879	9.6658
5	Adaptive histogram equalization	2.1358	15.0972
6	Principle Component Analysis	2.572	6.5945
7	Image Synthesis method	1.3892	38.006

15. Convex Hull

The convex hull of a set of points is the smallest convex set that contains the points. We represent a convex hull with a set of facets and a set of adjacency lists giving the neighbours and vertices for each facet. The boundary elements of a facet are called ridges. Each ridge signifies the adjacency of two facets. In R^3 and general position, facets are triangles, and ridges are edges.

A region is convex if any two points of the region are visible to one another within the region.

In other words, for any two points x and y in a convex region R, the line segment xy is also in R. Any point of the line segment xy can be written as $\alpha x+\beta y$, where $\alpha \geq 0$, $\beta \geq 0$, and $\alpha+\beta = 1$. So as α varies from 1 to 0, β varies in lock-step from 0 to 1, and the point moves along the segment xy, starting at x and ending at y.

This idea can be generalized to an arbitrary number of points: A convex combination of points $P = \{p_1, \ldots, p_n\}$ is of the form of equation 1.

$$\lambda_1 p_1 + \ldots\ldots + \lambda_n p_n, \tag{64}$$

where $\lambda_i \geq 0$ and $\sum \lambda_i = 1$. In some sense, the set of convex combinations tries to capture visibility from all points in the set S.

Given a set of distinct points P, we can visualize the convex hull intuitively: if each point of S is a nail pounded into the plane, the convex hull is the region enclosed by an elastic rubber band stretched around all the nails [1]. The convex hull of P, denoted by conv(P), is the intersection of all convex regions that contain P. Hence a convex hull can be defined as below,

For a point set $P = \{p_1, \ldots, p_n\}$, the convex hull of P is the set of all convex combinations of P.

The proof of this statement is divided into two parts.

Let M be the set of convex combinations of P. Formally,

$$M = \{\lambda_1 p_1 + \ldots\ldots + \lambda_n p_n | \lambda_i \geq 0, \sum \lambda_i = 1\}. \tag{65}$$

16. Quickhull Algorithm

We use quickhull algorithm to construct convex hull for the given points. The algorithm is as follows. We assume that the input points are in general position so that their convex hull is a simplicial complex. A simplicial complex is a topological space of a certain kind, constructed by "gluing together" points, line segments, triangles, and their n-dimensional counterparts

[2]. A simplicial complex $\mathcal{K}$ is a set of simplices that satisfies the following conditions:1. Any face of a simplex from $\mathcal{K}$ is also in $\mathcal{K}$. 2. The intersection of any two simplices $\sigma_1, \sigma_2 \in \kappa$ is a face of both $\sigma_1$and σ_2. A simplex (plural simplexes or simplices) is a generalization of the notion of a triangle or tetrahedron to arbitrary dimension. We represent a d-dimensional convex hull by its vertices and (d - 1)-dimensional faces (the facets). A point is extreme if it is a vertex of the convex hull. Each facet includes a set of vertices, a set of neighboring facets, and a hyperplane equation. A hyperplane is a generalization of the plane into a different number of dimensions. The (d - 2)-dimensional faces are the ridges of the convex hull. Each ridge is the intersection of the vertices of two neighboring facets. Quickhull uses two geometric operations: oriented hyperplane through d points and signed distance to hyper plane. It represents a hyperplane by its outward-pointing unit normal and its offset from the origin. The signed distance of a point to a hyperplane is the inner product of the point and normal plus the offset. The hyperplane defines a halfspace of points that have negative distances from the hyperplane. If the distance is positive, the point is above the hyperplane. Since a facet is linked to its neighbors, locating one visible facet allows the rest to be located quickly. The boundary of the visible facets is the set of horizon ridges for the point. A facet is visible if the point is above the facet .After initialization; Quickhull assigns each unprocessed point to an outside set [3]. By definition, the corresponding facet is visible from the point. When Quickhull creates a cone of new facets, it builds new outside sets from the outside sets of the visible facets. This process, called partitioning, locates a visible new facet for each point. If a point is above multiple new facets, one of the new facets is selected. If it is below all of the new facets, the point is inside the convex hull and can be discarded.

Steps in algorithm:

(i) First we create a simplex of d+1points. For each facet F and for each unassigned point p if point p is above the facet F, p is assigned to F's outside set.

(ii) For each facet F with a non empty outside set select the furthest point p of the F's outside set. Initialize the visible set V to F. For all unvisited neighbors N of the facets in V, if p is above N, add N to V.

(iii)The boundary of V is the set of horizon ridges H for each ridge R in H, fore each ridge R in H create a new facet from R and p. the n link the new facet to its neighbors.

(iv)For each new facet F for each new unassigned point q in an outside set of a facet in V if q is above F', assign q to F's outside set.

(v) Delete the facets in V and follow the step (iv) again until all facets in F are completed.

This outside set is the convex hull of the set of points.

17. Triangulation

For a point set S, the term edge is used to indicate any segment that includes precisely two points of S at its endpoints.A triangulation of a planar point set S is a subdivision of the plane determined by a maximal set of noncrossing edges whose vertex set is S.

The word maximal in the definition indicates that any edge not in the triangulation must intersect the interior of at least one of the edges in the triangulation. Triangulation is also defined a cell complex that subbdivides the convex hull of the sampling. If the sampling fulfills certain non-degeneracy conditions then all faces in the triangulation are simplices and the triangulation TD(S) is unique. The combinatorial and algorithmic complexity of the triangulation grows exponentially with the dimension of the embedding space of the original surface. The sampling S is said to be in general position if there are no degeneracies of the following kind: no three points on a common line, no four points on a common circle or hyperplane and no five points on a common sphere. In the following we always assume that the sampling S is in general position. We make the general position assumption only to keep the exposition simple.

For a point set S, a triangulation of S, denoted DT(S), is a triangulation that only has legal edges.

Conditions for Triangulation

For the set of boundary points S we have a triangulation DT(S), such that

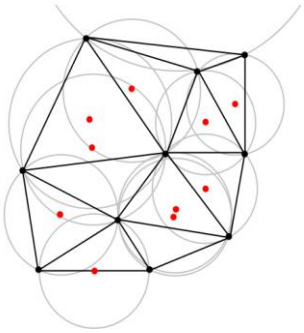

Figure 37. The triangulation DT(S) with all the circum circles and their centers shown in red

(i) Triangulation must satisfy empty sphere condition, that is, no point should lie inside the circum circle of any triangle from the set DT(S). This is tested using incircle test. This is shown in Figure 37.

(ii) One triangulation from all the possible triangulations of the set of points S, with the largest minimal internal angle of each triangle.

Triangle Construction

Given a set S of points, pick randomly a point p in S and search for one of the nearest neighbors q of p which create an edge pq such that no point lies inside the circle passing through pq. Now the task is to search a third point r such that pqr defines one triangle of the Triangulation DT(S).

Theorem: A third point r is defined in either side of the plane created by pq such that it should minimize Rcosγ. The Figure 38 shows the orientation of the 3 points.

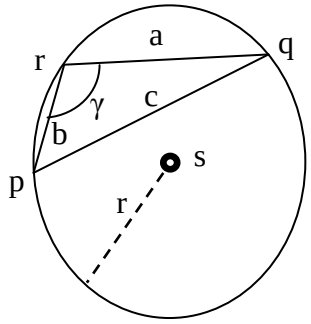

Figure 38: Circle containing the 3 points

For a third point r in S, let A be the area of the Δpqr. From geometry, we can see that

$$\cos\gamma = \frac{a^2 + b^2 - c^2}{2ab} \tag{66}$$

$$R = \frac{abc}{4A} \tag{67}$$

Now, we have to find a point r which will minimize the following equation.

$$R\cos\gamma = \frac{c(a^2 + b^2 - c^2)}{8A} \tag{68}$$

The area A of a triangle pqr can be conveniently expressed by the three-point determinant D(p;q;r) as

$$\begin{vmatrix} x_p & y_p & 1 \\ x_q & y_q & 1 \\ x_r & y_r & 1 \end{vmatrix} = x_p y_q + x_r y_p + x_q y_r - x_p y_r - x_q y_p - x_r y_q \tag{69}$$

from which the area of the triangle can be expressed as

$$A = \frac{1}{2 \mid D(p;q;r) \mid} \tag{70}$$

Note that the value of D (p; q; r) can be positive, negative or zero. Therefore, depending on the value of D (p; q; r), the third point of a triangle in DT(S) can be identified as :

Let r Є S/ {p; q} be the first point for which D (p; q; r) ≠ 0 and define K (p; q; r) as.

$$K(p;q;r) = \frac{a^2 + b^2 - c^2}{D(p;q;r)} \tag{71}$$

If D (p; q; r) > 0, identify the third point which minimizes K (p; q; r) or vice versa. If the three points are collinear, then D (p; q; r) = 0 and we can connect the points in a sorted order.

After the third point determination we check whether the triangle satisfies condition (i) or not using incircle test.

Incircle Test

To determine whether a point t lies inside the ΔPQR we perform a simple incircle test. The point t lies inside the ΔPQR if the following determinant is negative. The point lies on the circumcircle of the ΔPQR if the determinant is zero. The point lies outside the triangle if the determinant is greater than zero.

$$incircle(p;q;r;t) = \begin{vmatrix} p_x & p_y & p_x^2 + p_y^2 & 1 \\ q_x & q_y & q_x^2 + q_y^2 & 1 \\ r_x & r_y & r_x^2 + r_y^2 & 1 \\ t_x & t_y & t_x^2 + t_y^2 & 1 \end{vmatrix} > 0 \tag{72}$$

The incircle test in 2D in fact determines whether the projection of point t on the paraboloid $z=x^2 +y^2$ lies above, on or below the plane defined by the projection of p;q and r on the same paraboloid. Explanation on a 1D example is given in the Figure 39.

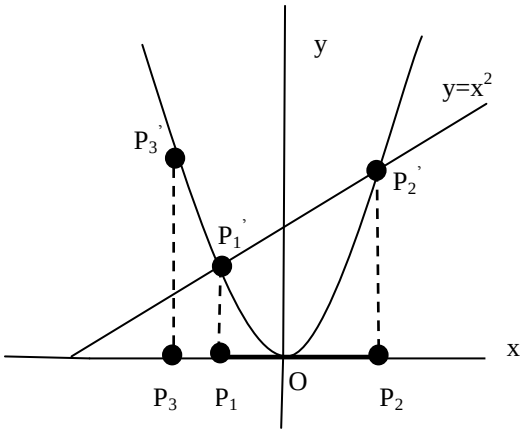

Figure 39:1D example of the incircle test

In this case, the test computes whether the point P_3 lies within the interval determined by points P_1 and P_2 by determining the position of its projection against the line given by the projection P_1' and P_2' of P_1 and P_2, respectively, on the parabola $y=x^2$.

18. Sphere Spinning Algorithm based on Triangulation

This algorithm is applied after the construction of Triangles described in previous section. We begin with a triangle which is circumscribed by a sphere of radius r. Choosing an edge of this triangle we rotate the sphere until it touches another point of the data sample. Now new triangle is formed from these new set of vertices. Let us consider a consider a surface of the three dimensional which contains large number of sample points so that sphere cannot pass through the surface without touching sample points. We start by placing a sphere of radius r in contact with three sample points. Keeping the sphere in contact with two of these initial points, we roll the spherel until it touches another point. We roll around each edge of the current mesh boundary. The points that the sphere touches form new triangles. The set of triangles formed while the sphere rolls on the surface constitutes the surface of the three dimensional object.

19. Algorithm for Surface Reconstruction

1. Separate the z coordinates form all the sampled points so as to project them on to the xy plane.
2. Now raise all the 2d points to 3d points by taking the z coordinates of the new points as x^2+y^2.
3. Construct the convex hull for all these points using quickhull algorithm.

4. Once the convex hull is obtained the points are brought down to 2d by removing the added third coordinate. By doing this we obtain the triangulation of all the points.
5. Now the original z coordinates are added to the points and obtained triangulation is plotted to get the reconstructed surface.

The accuracy of the surface obtained by this algorithm depends on the number of points considered. As the number of points increase the surface obtained by this algorithm becomes more accurate.

20. Results

The image obtained from Sonar which contains noise is shown in figure 40. The boundaries of the detected object are shown in figure 41. In this paper eight sonar images are taken and the boundaries of the eight images are extracted. These points are used to for 3D surface reconstruction based on Slice centroid method, Ball Pivoting method and Quick Hull and triangulation method.

3D construction based on Slice centroid method

The Fig. 8 represents the reconstruction of 3D irregular underwater images from the 2D slices obtained from Chirp technology SONAR Fig. 40. Here coordinates of the slice are X, Y and the level of the slices represents the Z-coordinate. The parameters are needed to uniquely describe the position of a point. These parameters are the azimuth θ, the altitude z. From these the 3d shape is obtained by fixing the altitude z and by varying angle (θ) varies from 0^0 to 360^0 (with an interval of 10^0). The azimuth (θ) is an angle made with X axis connecting given point and the origin of the coordinate axis and altitude z varies at different levels. The slices of 2D underwater images are given in Fig. 41.

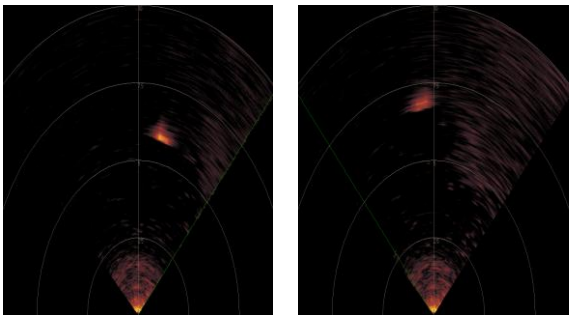

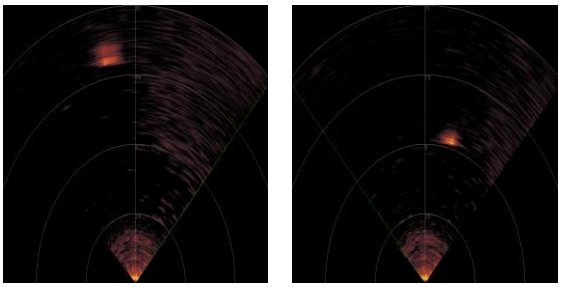

Fig. 40 2D Underwater SONAR images

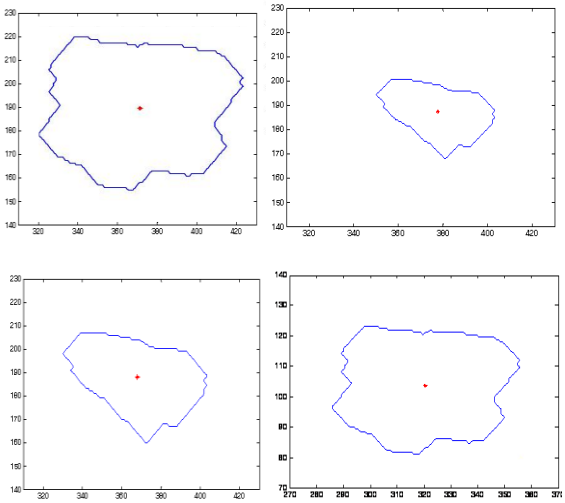

Fig. 41 Slices of 2D Underwater SONAR images

3D construction based on Sphere spinning algorithm

Total number of triangles formed is 2, 342. Now over these triangles, a sphere of radius r is rolled so as to find out the new triangles of the surface which are not found in triangulation. The result is shown in Figure 42.

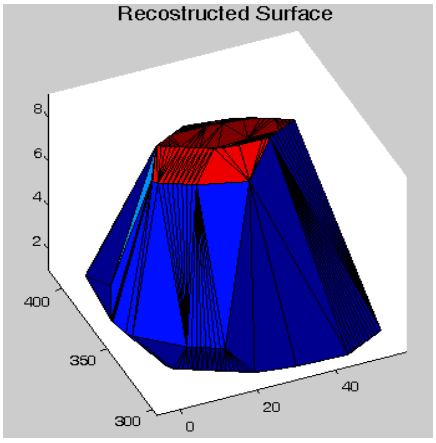

Fig. 42 Reconstruction of the object by rolling the sphere over the triangles

3D construction based on Quick Hull and Triangulation

Total number of triangles formed is 2, 342. Then the result obtained from triangulating the points of Sonar images is shown in the Figure 43. And the same process is done for the object which is farther from the Sonar and its result is shown in figure 44. The results clearly says that the object closer to Sonar has more resolution than the object farther from the Sonar as the Sonar beam width increases when the distance between the object and sonar increases.

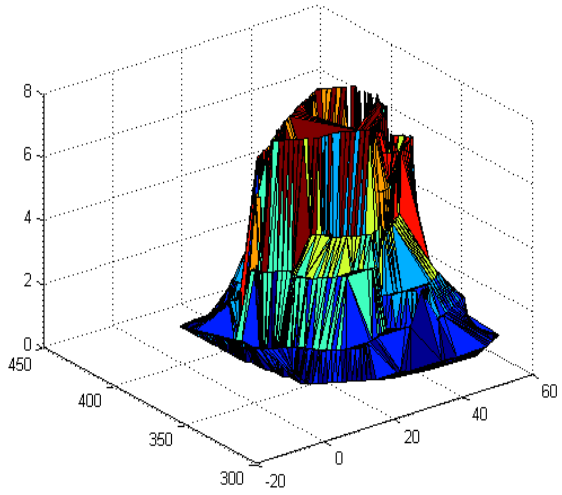

Fig. 43 Reconstruction of the object when it is closer to sonar

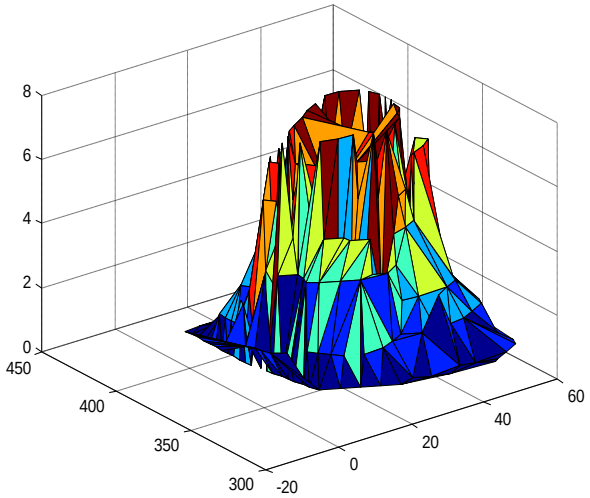

Fig. 44 Reconstruction of the object when it is farther to sonar

21. Conclusion

Unlike radar which is based on EM wave propagation, sonar is based on the principle of sound energy. Water is a good medium for propagating sound wave, however it propagates much slower than the RF waves in air, because the sound wave propagation is effected by several underwater characteristics like velocity of sound wave, sound pressure and power, transmission loss, absorption, viscosity, ionic relaxation and scattering. Sound waves while propagating underwater they get attenuated due to the cylindrical and spherical spreading of the energy. The transmission loss increases linearly in both spherical and cylindrical spreading and the transmission loss of spherical spreading is twice the transmission loss of cylindrical spreading. For example the transmission loss due to spherical spreading and cylindrical spreading at 100 m range are -46.0 dB and -23.0 dB respectively. The effects of various underwater characteristics on the sonar range equation are investigated.

Sonar is the only navigational aid used for AUV, submarine navigation. The modern AUVs use chirp technology based sonar for detecting the objects through the imaging of surveillance area. The pulse compression technique and different windowing techniques have been analyzed to check their impact on detecting the peak of the received signal. The range resolution characteristics of fixed frequency pulse sonar and chirp technology based sonar have also been investigated. It is concluded that the range resolution of chirp technology based sonar is 7.5mm and is 5 times better than the fixed frequency pulse sonar. The performance of various windowing techniques that suits the pulse compression of chirp technology sonar is investigated. It is concluded that the Blackman-Harris window performs better with a maximum side lobe level of 71dB and side lobe roll-off rate of 60 dB/decade.

The sonar often gives the data output in the form of videos, which are later converted to images for further processing. The statistical parameters useful for performance analysis of any specific image processing technique have been discussed and the values of these statistics derived for a underwater image are tabulated. Several existing image segmentation methods such as Adaptive thresholding, Edge detection based on difference technique, Canny edge detection, FCM thresholding and Adaptive histogram equalization have been implemented on the sonar images obtained from the imaging sonar. The PSNR values of these methods are 0.3037 dB, 13.4538 dB, 12.6053 dB, 9.6658 dB and 15.0972 dB respectively. It has been observed that even after processing the images using these methods the underwater noise is not eliminated completely from the images.

In order to eliminate the noise completely from the segmented images, the segmented images are combined into a single image, in such a way that the important features of the individual images are retained. This has been accomplished by using Principal Component Analysis. However even after applying PCA, the noise has not been eliminated completely. Therefore, a new Image Synthesis algorithm is developed. The criteria 'Peak Signal to Noise Ratio' (PSNR) has been used for evaluating the performance of existing image segmentation algorithms, PCA and along with the developed one. The PSNR values of Adaptive thresholding, Edge detection based on difference technique, Canny edge detection, FCM thresholding, Adaptive histogram equalization and PCA are 0.3037 dB, 13.4538 dB, 12.6053 dB, 9.6658 dB, 15.0972 dB and 6.5945 dB respectively. It has been observed that the PSNR of the developed algorithm is 38.006 dB which is better than the existed methods, thereby concluding that the algorithm that has been developed is far superior to those existing ones.

The objects that are detected using above image processing methods are in the form of two dimensional images which provides only range and bearing but not the depth of the object. For extracting the 3D features from the 2D data three surface reconstruction algorithms namely Slice centroid algorithm, Ball Pivoting algorithm and Triangulation are developed in this thesis. The first algorithm is developed based on concept of spherical co-ordinates inorder to obtain the 3D shape. In the second algorithm surface is constructed by rolling a sphere over the edges of triangles formed. In third algorithm the surface is constructed by forming triangles from the data points obtained from the sonar scans based on quick hull algorithm. The triangulation is done by constructing the convex hull of the 2D data using Quickhull algorithm. It has been observed that among all three methods the method 'Triangulation based on quick hull algorithm' performs well in constructing the 3D surface with good resolution where the resolution is based on the number of triangles so constructed. In Triangulation based on quick hull algorithm, 2342 triangles are formed to construct the surface of the object whereas in Ball Pivoting algorithm only 163 triangles are formed. It has also been observed that there is a resolution difference between the object reconstructed when the sonar is nearer and farther with respect to the object. While reconstructing the surface for object nearer to the sonar, the triangles formed are 2342 whereas for object farther to the sonar the triangles formed are 576.

References:

1. Alexander Barvinok. A Course in Convexity. American Mathematical Society, 2002.
2. Bernd Jahne, Practical Handbook on Image Processing for Scientific and Technical Applications, Second edition, CRC Press, Boca Raton, United States, ISBN: 0-8493-1900-5, 2004.
3. Bell J.M., Dura E., Reed S., Petillot Y.R., and Lane D.M., "Extraction and Classification of Objects from Sidescan Sonar", IEE Workshop on Nonlinear and Non-Gaussian Signal Processing, 8-9th July 2002.
4. Bell J.M., Dura E., Reed S., Petillot Y.R., and Lane D.M., "Extraction and Classification of Objects from Sidescan Sonar", IEE Workshop on Nonlinear and Non-Gaussian Signal Processing, 8-9th July 2002.
5. Cox I. J., Roy S., and Hingorani S. L., "Dynamic histogram warping of image pairs for constant image brightness", in Proceedings of the IEEE International Conference on Image Processing, pp. 366–369, 1995.
6. Chantler M. J. and Stoner J. P., "Automatic interpretation of sonar image sequences using temporal feature measurements", IEEE Journal of Ocean Engineering, vol.22, Issue 1, pp: 47–56, 1997.
7. Cushieri J. and Negahdaripour S., "Use of forward scan sonar images for positioning and navigation by an AUV", in Proceedings of OCEANS'98, Nice, France, (IEEE/OES, Ed.), Vol. 2, pp:752–756, September 1998.
8. Dougherty Edward R., Mathematical Morphology in Image Processing, CRC Press, 1993.
9. Dong-Hoon Yang, Ji-Wook Kwon and Suk-Kyo Hong, "A Collision Avoidance Algorithm for Two Mobile Robots with Independent Goals in RoadMap", School of Electrical and Computer Engineering, Ajou University, International Joint Conference Oct. 2006 page(s): 3053-3058.
10. Doucette J., Navigation Autonomous Underwater Vehicles, http://www.whoi.edu/ oceanus/ viewImage.do? id=19010&aid=9207. [Accessed December 10,2008].
11. Dolbec M., "Velocity Estimation Using Forward Looking Sonar", M.S. Thesis, Naval Postgraduate School, 2007.
12. Deutsch R., "Estimation Theory", Prentice-Hall, Englewood Cliffs, New Jersey, 1965.
13. Fausto Bernardini, Joshua Mittleman, Holly Rushmeier, Claudio Silva, "The Ball-Pivoting Algorithm for Surface Reconstruction", IEEE Transactions on Visualization and Computer Graphics, Vol. 5, No. 4, October-December 1999.
14. Foresti G. L., Murino V., Regazzoni C. S. and Trucco A., "A voting-based approach for fast object recognition in underwater acoustic images", IEEE Journal on Ocean Engineering, Vol. 22, No.1, pp: 57–65, 1997.
15. Fisher R., Dawson-Howe K., Fitzgibbon A., Robertson C. and Trucco E., Dictionary of Computer Vision and Image Processing, John Wiley, ISBN 0-470-01526-8, 2005.
16. Fox W. L. J., Hsieh J. and Polwarth C., "Segmentation of images from an acoustic lens sonar", MTTS/IEEE TECHNO-OCEAN '04, Vol.4, pp: 2029– 2035, 2004.
17. Franco Preparata and Michael Shamos. Computational Geometry: An Introduction. Springer-Verlag, 3rd edition, 1990.
18. Gonzalez R. C., Woods R. E. and Eddins S. L., Digital Image Processing using MATLAB, Pearson Education, 3rd edition, 2005.
19. H.B. Mitchell, "Image Fusion", Springer, 2010.
20. Howard Anton, "Elementary Linear Algebra 5e", Publisher John Wiley & Sons Inc., Jan 2006.
21. Jun Zhang, "Face recognition: Eigenface, Elastic matching and neural nets", Proceeding s of the IEEE, Vol. 85, No.9, September 1997.

22. Joseph O'Rourke. Computational Geometry in C. Cambridge University Press, 2nd edition, 1998.
23. Jon Mc Cammond., "Noncrossing partitions in surprising locations" American Mathematical Monthly, Volume 113, pages 598–610, 2006.
24. Lindsay I Smith, "A tutorial on Principal Components Analysis", February 26, 2002
25. Leick A., GPS satellite surveying, Third edition, John Wiley and Sons, USA., 2004.
26. G. Sasi Bhushana Rao, M.N.V.S.S.Kumar, 'A New Image Segmentation Thresholding Technique for Precise processing of Sector Scan SONAR images', National Symposium on Acoustics NSA-09, Nov 26-28, 2009 at RCI, Hyderabad.
27. G. Sasi Bhushana Rao and M N V S S Kumar, "QAA Based Underwater Targets Detection", Advances in Communication Technologies (NCACT-12), January 9th -10th 2012.
28. Mei Han, Wei Xu, Hai Tao and Yihong Gong, "An algorithm for multiple object trajectory tracking Computer Vision and Pattern Recognition", Proceedings of IEEE Conference on Computer Society, Vol.1, pp:I-864 - I-871, 27 June-2 July 2004.
29. M N V S S Kumar and G. Sasi Bhushana Rao, "A New Algorithm for 3D Surface Reconstruction from Point Clouds obtained from 2D Sonar Images Using Triangulation", NAVCOM-2012, Osmania University, Hyderabad, December 19th – 20th, 2012.
30. Mignotte M., Collet C., Perez P., and Bouthemy P., "Statistical model and genetic optimization: application to pattern detection in sonar images", In Proceedings of IEEE International Conference Acoustics, Speech and Signal Processing, Vol.5, pp:2741–2744, 1998.
31. M N V S S Kumar and G. Sasi Bhushana Rao, "Development of Image Synthesis Algorithm for Detecting Underwater Targets from SONAR Images", National IETE Conference on Advanced Communication and Computer Technologies, July 6th – 7th , 2012.
32. Martinez G., "Criterion for automatic selection of the most suitable maximum likelihood thresholding algorithm for extracting object from their background in a still image," in Proceedings of IAPR Conference on Machine Vision Applications, Tsukuba, Japan, May 16-18 2005.
33. G. Sasi Bhushana Rao and M N V S S Kumar, "Development of Image Fusion Algorithm for Detection of Underwater Targets from SONAR Images", Advances in Communication, Navigation and Computer Networks (ACNCN-2012), March 17th – 12th, 2012.
34. Meyroqitz A. L., Blidberg D.R. and Michelson R.C., "Autonomous vehicles", In Proceedings of the IEEE, Vol.84, No.8, pp: 1147-1164, August 1996.
35. Marshall Bern. Triangulations. In Jacob E. Goodman and Joseph O'Rourke, editors, Handbook of Discrete and Computational Geometry, chapter 25, pages 563–582. CRC Press LLC, 2nd edition, 2004.
36. M N V S S Kumar ,G Sasi Bhushana Rao, "Surface Reconstruction of 3D Underwater Object from 2D Images obtained from Sector Scan Sonar fitted on AUV", Journal of Communication, Navigation and Signal Processing, 2nd Issue, Vol. 1, July 2012.
37. Quidu I., Malkasse P., Burel G., and Vilbe P., "Mine classification using a hybrid set of descriptors", Proceedings of the Oceans 2000 MTS/IEEE Conference and Exhibition, Vol.1, pp:291–297, 2000.
38. Qihu Li, "Digital Sonar Design in Underwater Acoustics", Springer Heidelberg Dordrecht, 2012.
39. Qu, G., Zhang, D., Yan, P.: Information measure for performance of image fusion. Elect. Lett. 38, 313–315 (2002)

40. Russell B., Torralba A., Murphy K., and Freeman W. T., "LabelMe: a database and web-based tool for image annotation. International Journal of Computer Vision, Vol.77, No.1, pp:157-173, May 2008.
41. Raimund Seidel. Convex hull computations. In J. E. Goodman and J. O'Rourke, editors, Handbook of Discrete and Computational Geometry, chapter 22, pages 495–512. CRC Press LLC, 2nd edition, 2004.
42. Sohi, D.S., Devgan, S.S., "Application to enhance the teaching and understanding of basic image processing techniques", Proceedings of the IEEE pp: 413 – 416, 7-9 April 2000.
43. Satya Swaroop Pradhan, Dipti Patra, Pradipta Kumar Nanda, "Adaptive Thresholding Based Image Segmentation with Uneven Lighting Condition", Proc. on IEEE Region 10 Colloquium and the Third ICIIS, Kharagpur, INDIA, 8-10 December, 2008.
44. Sasibhushana Rao G., Global Navigation Satellite Systems (GNSSs) with essentials of Satellite Communication, May 2010.
45. Satyan L. Devadoss, Joseph O'Rourke, "Discrete and Computational GEOMETRY", Princeton University Press, 2011.
46. Tommasini T., Fusiello A., Trucco E. and Roberto V., "Making good features track better Computer Vision and Pattern Recognition", Proceedings IEEE Conference on Computer Society pp:178 – 183, 23-25 June 1998.
47. Tim Morris, Computer Vision and Image Processing, Palgrave Macmillan, ISBN 0-333-99451-5, 2004.
48. Tu, T.-M., Su, S.-C., Shyu, H.-C., Huang, P.S.: A new look at IHS-like image fusion methods. Inf. Fusion 2, 177–186 (2001)
49. Urick R. J., Principles of Underwater Sound, 3rd edition, New York, McGraw-Hill, 1983.
50. Waite A.D., SONAR for Practising Engineers, 3rd edition, John Wiley & Sons Ltd., 2002.
51. Wang, Z., Bovik, A.C., Sheikh, H.R., Simoncelli, E.P.: Image quality assessment: From error visibility to structural similarity. IEEE Trans. Image Process. 13, 600–612 (2004)
52. Xu L., Landabaso J. L. and Lei, B., "Segmentation and tracking of multiple moving objects for intelligent video analysis", BT Technology Journal.
53. Yi Zhou, "Principal Component Analysis Based Image Fusion Routine with Application to Stamping Split Detection", Clemson University, USA, 2010.
54. Zerr B., Mailfert G., Bertholom A. and Ayreault H., "Sidescan sonar image processing for AUV navigation", Oceans 2005 - Europe, Vol.1, pp. 124-130, 20-23 June 2005.

List of Publications related to work:

1. M N V S S Kumar, G Sasibhushana Rao, L Ganesh, "A Heuristic 3D Construction Algorithm for Detection of Tumour in Magnetic Resonance Imaging Slices", International Conference on Hybrid and Composite Materials,chemical processing:HCMCP-2016, St.Peter's Engineering College, Hyderabad, Sep 25-27, 2016.
2. M N V S S Kumar, G.Sasibhushana Rao, L.Ganesh, Rajkumar Goswami, "Expectation-Maximization based image fusion algorithm for detection of Underwater targets from SONAR images", Elsevier International Conference on Computational Modeling and Security, Bangalore, pp: 762-769, Feb-2016. (Procedia Computer Science Journal).
3. M. N. V. S. S. Kumar, "A new approach for tracking moving objects in underwater environment", CURRENT SCIENCE, VOL. 110, NO. 7, 10 APRIL 2016, doi: 10.18520/cs/v110/i7/1315-1323
4. M N Mani, G S Rao, K S Prasad, L Ganesh, M N V S S Kumar, "A new method of target tracking by EKF using bearing and elevation measurements for underwater environment", Robotics and Autonomous Systems, Elsevier, August 2015.
5. M.N.V.S.S Kumar, "3D Construction of Tumour in Magnetic Resonance Imaging Slices", CIIT Journal of Digital Image Processing, Vol 8, No 9, 0974 – 9691, Oct, 2016.